Université Mohamed Khider de Biskra
Sciences exactes et sciences de la nature et de la vie
Sciences de la matière

MÉMOIRE DE MASTER

Sciences de la matière
La physique
Physique de l'énergie et énergies renouvelables

Réf. : ……………………………………...

Présenté et soutenu par :
Ben amara afifa
Soltan zohra
Le : 20-9-2020

Numerical simulation of CZTSSe tandem solar cell

Jury :

Boumaraf Rami	M.C. «B»	Université Med Khider - Biskra	President
NadiaMessei	M.C. «B »	Université Med Khider - Biskra	Superviseuse
Boudhib wahiba	M.A.A	Université Med Khider - Biskra	Examiner

Année universitaire : **2019/2020**

Abstract:

    In this work, **CZTSSe /Si** tandem solar cell was studied using the wxAMPS3 simulation tool. First CZTS and c-Si solar cells were simulated separately, the thickness of CZTS absorber layer was optimised and we tested the effect of CZTSSe gap-energy on cell parameters. Next we stacked the two cells to create CZTSSe/Si tandem. In this part we have studied again the effect of CZTSSe gap on tandem parameters (J_{sc},V_{oc},FF and the efficiency). As results of this work we can say that tandem structure gives better efficiency.

At Eg_{CZTSSe}=1.5eV the efficiency of the tandem is 25% while it is 15.73% and 13.05% for CZTSSe and Si cells respectively. The results show that the higher Eg $_{CZTSSe}$ value gives the better parameters of the tandem.

Key words: CZTSSe; Si; solar cell; tandem; wxAMPS.

ملخص:

    في هذا العمل ، تمت دراسة الخلايا الشمسية الترادفية Si / CZTSSe باستخدام أداة محاكاة wxAMPS3. تمت محاكاة الخلايا الشمسية CZTS و c-Si الأولى بشكل منفصل ، وتم تحسين سماكة الطبقة الماصة CZTS واختبرنا تأثير فجوة الطاقة CZTSSe على معلمات الخلية. بعد ذلك قمنا بتكديس الخليتين لإنشاء ترادف CZTSSe / Si. في هذا الجزء درسنا مرة أخرى تأثير فجوة CZTSSe على (Jsc ، Voc، FF والكفاءة) . نتيجة لهذا العمل يمكننا القول أن الهيكل الترادفي يعطي كفاءة أفضل.

عند EgCZTSSe = 1.5eV ، تبلغ كفاءة الترادف 25٪ بينما تبلغ 15.73 و 13.05٪ لخلايا CZTSSe و Si على التوالي. تظهر النتائج أن قيمة Eg CZTSSe الأعلى تعطي أفضل كفاءة.

الكلمات المفتاحية : Si ; CZTSSe;الخلايا الشمسية ; ترادف ; wxAMPS . ;

Abstract:

    Dans ce travail, la cellule solaire tandem CZTSSe / Si a été étudiée à l'aide de l'outil de simulation wxAMPS3 .Tout d'abord, les cellules solaires CZTS et c-Si ont été simulées séparément, l'épaisseur de la couche d'absorbeur CZTS a été optimisée et nous avons testé l'effet de l'énergie de gap CZTSSe sur les paramètres de la cellule. Ensuite, nous avons empilé les deux cellules pour créer un tandem CZTSSe / Si. Dans cette partie, nous avons à nouveau étudié l'effet du gap CZTSSe sur les paramètres du tandem (Jsc, Voc, FF et le rendement). Comme résultat de ce travail, nous pouvons dire que la structure en tandem donne un meilleur rendement.

A EgCZTSSe = 1,5eV, l'efficacité du tandem est de 25% alors qu'elle est de 15,73% et 13,05% pour les cellules CZTSSe et Si respectivement. Les résultats montrent que la valeur Eg CZTSSe la plus élevée donne les meilleurs paramètres du tandem.

Mots clés : CZTSSe ; Si; cellule solaire; tandem; wxAMPS

Acknowledgement

First, we would like to thank our advisor Dr. Nadia Messei for his valuable guidance and support during our dissertation and we are benefited a lot from her profound knowledge.

It was a very nice experience to work with her.

Also, I would like to thank all members of the examining committee of this letter.

Thank you, Hadger, and hala for being by my side every time I need it to prepare the letter.

Dedication

we dedicate this work to the best parents

To our brothers and sisters

Table of contents

viii

Introduction

The solar, wind, and thermal energies are normally come under the umbrella of the renewable energy, which is one of the alternatives to the conventional energy. The hydro, thermal by coal, and nuclear can be treated as conventional energy sources.The nuclear disasters of Chernobyl and Fukushima are cautioning world about dangers of nuclear plants and consequences to mankind.

An ongoing challenge facing scientists is to improve the efficiency of solar cells. To harvest the largest amount of sun energy possible, without increasing the cost. Until recently, solar cell technology was based on silicon, which effectively absorbs certain wavelengths of sunlight, leaving part of the solar energy untapped.

In recent years, a lot of efforts have been initiated to develop silicon solar cells. Obviously, we can play as much as we play alternately in silicon solar cells to improve their performance. The main disadvantage of Si solar cells are that they are indirect bandgap semiconductors and need a thick layer of about 180300 μm to absorb the photons [1]. The band gap of 1.1 eV for silicon absorbs no more than 50% of the visible spectrum, that is, the blue and green areas. These factors undermine to reduce the cost of Si solar cells.The search for suitable band gap materials for the applications of solar cells is essential. Therefore, scientists have initiated to fabricate novel and new absorbers by identifying the earth's abundant solar energy materials to reduce the cost of thin-film solar cells. Recently, $Cu(In1yGay)(S1xSex)2$ (CIGSS) based thin-film solar cells are technologically developed in which the Zn/Sn replaces In/Ga that reduces cost of the solar panels partially. The replacement changes the system from $Cu(In1yGay)(S1xSex)2$ to $Cu2(ZnSn)(S1xSex)4$. In every year, the cost of In or Ga doubles its original value owing to high demand in the market. In the earth crust, the existences of Cu, Zn, Sn, S, and Se are 50, 75, 2.2, 260, and 0.05 ppm,respectively where as availability of In is 0.049 ppm [2,3]. It is learned that 30 tons of In is necessary to produce 1 GW power [4,5,6].

In our work, we will use the wxAMPS3 software to simulate and study a CZTSS / Si-based double-link (Tandem) solar cell with the goal of optimizing the silicon cell. We will simulate the effect of thickness and band gap energy on the top cell of the tandem structure, thus this work will contribute to a better understanding and analysis of Tandem CZTSS / Si solar cells.

Chapter 1 provides an overview of solar PV cells and an explanation of the purpose of this work. The important principles and properties of semiconductors were reviewed.

Chapter 2 deals with the important properties of materials Si, CZTSS and an overview of the simulation program as wxAMPS3.

Chapter 3 Summarizes all simulation results and discussions in both cases, the effect of CZTSSe layer thickness and the Eg bandgap effect. First, we will examine the effect of CZTSSe layer thickness on the performance of our CZTSSe solar cell. Second, we will test the effect of the band gap on the performance of the CZTSSe cell. Third, we will simulate a Si solar cell. Finally we will synthesize the two CZTSSe / Si cells into a tandem cell and give a result.

References

[1] S. Mehta, IEEE Power Energ. Mag. 9 (2011) 94. Available from: http://dx.doi.org/ 10.1109/MPE.2011.940418.

 [2] M.I. Hossain, Chalcogenide Lett. 9 (2012) 231.

[3] H. Wang, J. Bell, The Fifth World Congress on Engineering Assest Management (WCEAM 2010), 2527 October 2010, Brisbane Convention and Exhibition Center, Brisbane, Queensland University of Technology.

[4] W. Thumma, et al., Proceedings of the World Conference on Photovoltaic Energy Conversion-1, Hawaii, 1994, p. 262.

[5] S. Ito, T.N. Murakami, P. Comte, P. Liska, C. Gratzel, M.K. Nazeeruddin, et al., Thin Solid Films 516 (2008) 4613.

[6] J. Emsley, The Elements, third ed., Oxford University Press, Oxford, 1998. p. 289.

Chapter I :

Solar Cells

I.1 Introduction

A solar cell, or photovoltaic cell, is an electrical device that converts the energy of light directly into electricity by the photovoltaic effect, which is a physical and chemical phenomenon. The solar cell is a PN junction, the operation of which is based on the absorption of solar luminous flux, generation and collection of charges.

At the beginning of this research, we will deal with a set of concepts that concern solar cells, including the constituent material, as well as the method of work, the generations of these cells and multijunction solar cell.

I.2 Solar Radiation

At the core of the Sun, nuclear fusion of hydrogen releases massive heat. The Sun is surrounded by a thin atmosphere which consists mostly of hydrogen atoms. This is the so-called photosphere that absorbs the heat and emits electromagnetic radiation into outer space with almost the same spectral radiation as that of a black body in thermal equilibrium at a high temperature Ts. According to Planck's formula, the power emitted per unit projected area of the black body into a unit solid angle per unit frequency interval is given by the spectral irradiance $L_v (T_s)$, defined

$$L_v(T_s) = \frac{2hv^3}{c^2} \frac{1}{exp(hv/k_bT_s) - 1} \qquad (\text{I.1})$$

where v is the frequency of radiation, cis the light speed, his the Plank constant, and $k_b$is the Boltzmann constant. The photon energy of electromagnetic oscillation at frequency vis given by hv. The solid angle $\Omega_s$of the Sun (in steradians) which is seen from the Earth is calculated as:

$$\Omega_s = \frac{\pi r^2}{R^2} = 6.79 \times 10^{-5} \qquad (\text{I.2})$$

where r is the radius of the Sun (i.e. 6.96×10^5 km) and Ris the mean orbital radius of the Earth rotating around the Sun (i.e. 1.496×10^8 km).

The spectral photon irradiance which is defined by the number $N_v(T_s)$ of incident photons per square meter per second per Hertz arriving at the top of the Earth's atmosphere is therefore expressed:

$$N_v(T_s) = \frac{\Omega_s L_v(T_s)}{hv} \quad . \qquad (\text{I.3})$$

The smooth curve shown in Figure (I.1) is the theoretical plot of $N_v(T_s)$ versus photon energy hv, evaluated by substituting the effective temperature T_s of the photosphere (which is assumed to be 5772 K) into Equation (I.3). The accuracy of this assumption is confirmed in Figure (I.1) as the theoretical curve for the electromagnetic wave emitted from a black body at T_s agrees quite well with the observed spectra of extra-terrestrial radiation in photon energy of 1.15−1.72 eV. The two curves also cross at 3.11 and 0.44 eV. The latter spectra are derived from those of AM0 radiation measured as a function of wavelength [1].

However, there is a significant difference in peak irradiance between the two curves. The total power of electromagnetic radiation which is perpendicularly incident on a unit area is called the solar constant C_s and is thus defined by:

$$C_s \int_0^\infty h\nu N_\nu (T_s) d\nu = \Omega_s \int_0^\infty L_\nu (T_s) d\nu = \frac{r^2 \sigma T_s^2}{R^2} \tag{I.4}$$

where σ is the Stefan-Boltzmann constant equal to 5.67×10^{-8}W m² k^{-4}. The effective surface temperature $T_s (= 5772$ K) of the Sun is determined such that the theoretical value
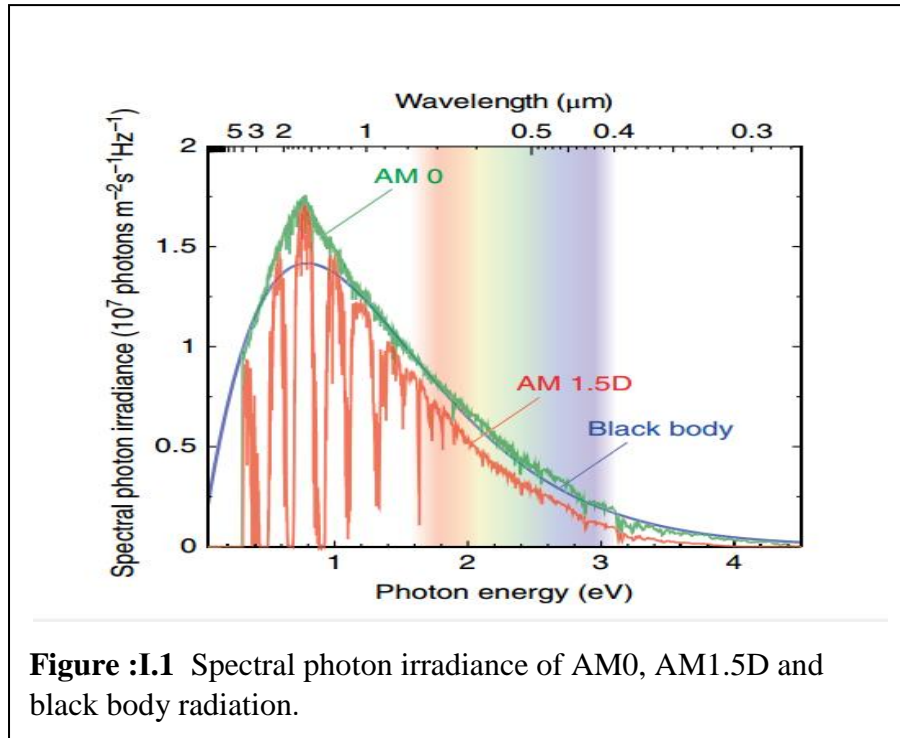
Figure :I.1 Spectral photon irradiance of AM0, AM1.5D and black body radiation.

I.3 History of solar cells

It has now been 175 years since 1839 when Alexandre Edmond Becquerel observes the photovoltaic (PV) effect via an electrode in a conductive solution exposed to light [2]. It is instructive to look at the history of PV cells [3] since that time because there are lessons to be learned that can provide guidance for the future development of PV cells.

Table I.1: 1839-Present :

Years	Events
• 1839	**- Alexandre Edmond Becquerel observes the photovoltaic effect via an electrode in a conductive solution exposed to light [2]**
• 1877	**- W.G. Adams and R.E. Day observed the photovoltaic effect in solidified selenium, and published a paper on the selenium cell [4]. 'The action of light on selenium,' in "Proceedings of the Royal Society, A25, 113**
• 1883	**- Charles Fritts develops a solar cell using selenium on a thin layer of gold to form a device giving less than 1% efficiency.**

•1928	– F. Bloch develops band theory based on single crystal periodic lattice [5].
•1931	A. H. Wilson develops theory of high purity semiconductor [6]
• 1948	- Gordon Teal and John Little adapt the Czochralski method of crystal growth to produce single-crystalline germanium and, later, silicon [7]
• 1957	- AT&T assignors (Gerald L. Pearson, Daryl M. Chapin, and Calvin S. Fuller) receive patent US2780765, "*Solar Energy Converting Apparatus*."[8] They refer to it as the "solar battery." Hoffman Electronics creates an 8% efficient solar cell.
• 1962	The Telstar **communications satellite is powered by solar cells [9].**
• 1970	- First highly effective GaAsheterostructure solar cells are created by ZhoresAlferov and his team in the USSR [10]
• 1978	US Public Utilities Regulation Act (PURPA) passed [11]
• 1990	– L. Fraas, J. Gee, k. Emery, et al describe the 35% efficient Two-Chip Stack GaAs/GaSb Concentrator Solar Cell [12].
• 1994	- NREL develops a GaInP/GaAs two-terminal concentrator cell (180 suns) which becomes the first monolithic two Junction solar cell to exceed 30% conversion efficiency [13].
• 1998	– Demonstration of First ThermoPhotoVoltaic Heat & Electricity Co-generation MidnightSun™ Stove by JX Crystals Inc [14]
• 2000	Germany's Renewable Energy Sources Act creates Feed-In-Tariff (FIT) for solar [15].
• 2004	K. Araki et al demonstrate 28% efficient CPV module [16]
• 2006	– L. Fraas et al demonstrate 33% efficient Dual Focus HCPV Module
• 2007	Construction of Nellis Solar Power Plant, a 15 MW PPA installation using SunPower- Corp modules
• 2011	- Fast-growing factories in China push manufacturing costs down to about $1.25 per watt for silicon photovoltaic modules. Installations double worldwide [17]
• 2013	– *Cumulated* world wide solar PV installations passes 100 GW [17]

I.4.Semiconductors

   A semiconductor material has an electrical conductivity value falling between that of a conductor, such as metallic copper, and an insulator, such as glass. Its resistance falls as its temperature rises, metals are the opposite. Its conducting properties may be altered in useful ways by introducing impurities ("doping") into the crystal structure[18]. The atoms in a semiconductor are materials from either group IV of the periodic table, or from a combination of group III and group V (called III-V semiconductors), or of combinations from group II and group VI (called II-VI semiconductors)[19] .Because different semiconductors are made up of elements from different groups in the periodic table, properties vary between semiconductors.Some examples of semiconductors are silicon, germanium, gallium arsenide, and elements near the so-called "metalloid staircase" on the periodic table. [18]

   Semiconductors, such as Silicon (Si) are made up of individual atoms bonded together in a regular, periodic structure to form an arrangement whereby each atom is surrounded by 8 electrons. An individual atom consists of a nucleus made up of a core of protons (positively charged particles) and neutrons (particles having no charge) surrounded by electrons. The number of electrons and protons is equal, such that the atom is overall electrically neutral. The electrons surrounding each atom in a semiconductor are part of a covalent bond. A covalent bond consists of two atoms "sharing" a pair of electrons. Each atom forms 4 covalent bonds with the 4 surrounding atoms. Therefore, between each atom and its 4 surrounding atoms, 8 electrons are being shared. The structure of a semiconductor is shown in the figure (I.2)[20] .

Figure :I.2 Schematic representation of covalent bonds in a silicon crystal lattice. Each line connecting the atoms represents an electron being shared between the two. Two electrons being shared are what form the covalent bond.
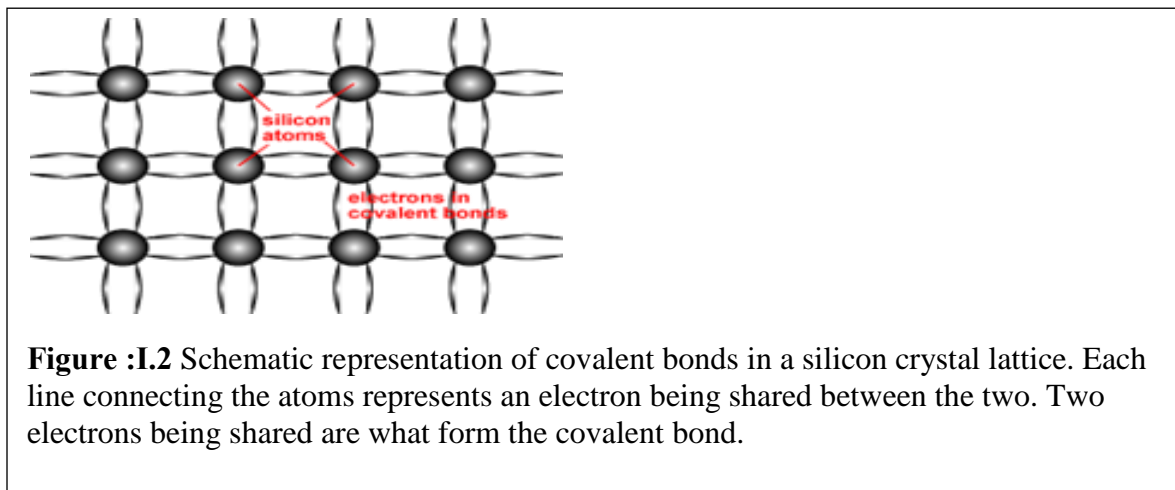
I.4.1 Band Gap

   The band gap of a semiconductor is the minimum energy required to excite an electron that is stuck in its bound state into a free state where it can participate in conduction. The band structure of a semiconductor gives the energy of the electrons on the y-axis and is called a "band diagram". The lower energy level of a semiconductor is called the "valence band" (EV) and the energy level at which an electron can be considered free is called the "conduction band" (EC). The band gap (EG) is the gap in energy between the bound state and the free state, between the

valence band and conduction band. Therefore, the band gap is the minimum change in energy required to excite the electron so that it can participate in conduction.[21]

Figure: I.3 Schematic of the energy bands for electrons in a solid.
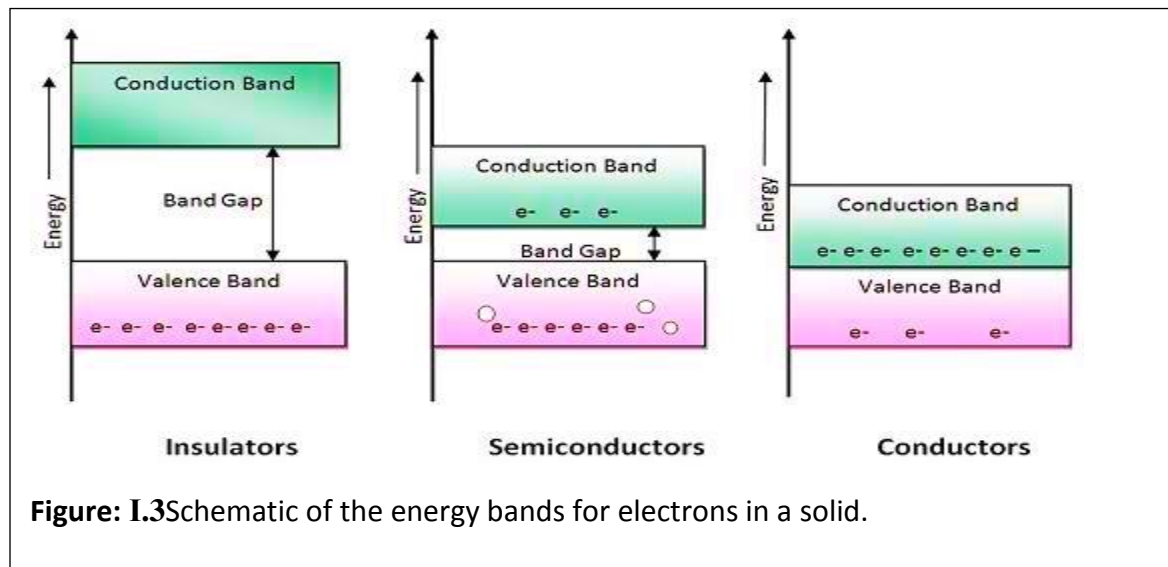
I.4.2 Fermi Energy and Holes

Of particular interest is the existence in semiconductors, at moderate temperatures such as room temperature, of the two energy bands that are partly filled. The higher of these two bands is mostly empty but a number of electrons exist near the bottom of the band, and the band is named the conduction band . The lower band is almost full; however, because there are empty states near the top of this band, it also exhibits conduction and is named the valence band. The electrons that occupy it are valence electrons, which form covalent bonds in a semiconductor such as silicon. Figure (I.4) shows the room temperature picture of a semiconductor in thermal equilibrium. An imaginary horizontal line at energy Ef, called the Fermi energy, represents an energy above which the probability of electron states being filled is under 50%, and below which the probability of electron states being filled is over 50%. We call the empty states in the valence band holes. Both valence band holes and conduction band electrons contribute to conductivity. [22]

Figure: I.4 Room temperature semiconductor showing the partial filling of the conduction band and partial emptying of the valenceband. The Fermi energy lies between the bands. Solid lines represent energy states that have a significant chance of being filled
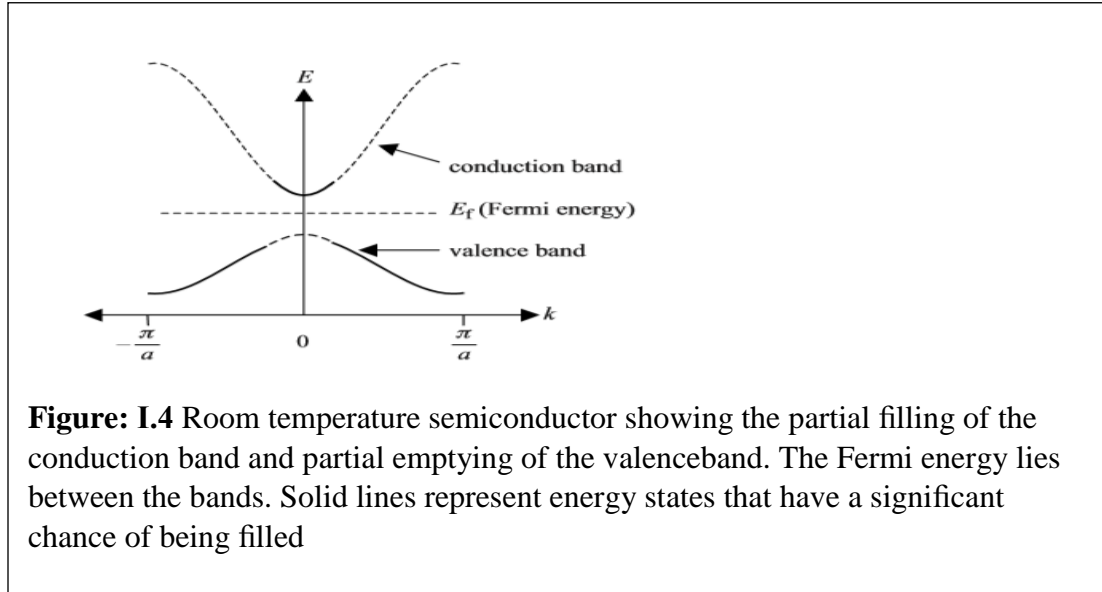
I.4.3 Electrons and Holes in a Semiconductor

In the broad temperature range of 'normal' temperatures the conduction band is 'almostempty' and the valence band 'almost full' of electrons. 'Almost empty' in the conduction band means that only a few electrons are in the permitted energy states all these states lie near the edge of the band, there still are numerous unoccupied states close to the occupied levels, so these electrons are capable of reaching a higher level by an almost continuous process[23]

I.4.4 Intrinsic Carrier Concentration

The effective density of states in the conduction band N_C is equal to $2(\frac{2\pi m_n KT}{h^2})^{\frac{3}{2}}$. Similarly, the effective density of states in the valence band N_V is $2(\frac{2\pi m_p KT}{h^2})^{\frac{3}{2}}$. At room temperature, N_C for silicon is 2.8 x 10^{19} atoms/cm^3.For an intrinsic semiconductor, the number of electrons per unit volume in the conduction band is equal to the number of holes per unit volume in the valence band. [24] That is,

$$n = p = n_i \tag{I.5}$$

where ni is the intrinsic carrier density. Since

$$n = N_C e^{(\frac{-(E_c - E_F)}{KT})} \tag{I.6}$$

and

$$p = N_V e^{(\frac{-(E_F - E_v)}{KT})} \tag{I.7}$$

where n is the electron density and p is the hole density

$$np = N_c N_v e^{(\frac{(E_v - E_c)}{KT})} = N_c N_v e^{(\frac{-Eg}{KT})} \tag{I.8}$$

Therefore,

$$n_i = (N_c N_v)^{\frac{1}{2}} e^{\left(\frac{-E_g}{2KT}\right)} \tag{I.9}$$

I.4.4.1 N-type semiconductors

N-type semiconductors are created by doping an intrinsic semiconductor with an electron donor element during manufacture. The term n-type comes from the negative charge of the electron. In n-type semiconductors, electrons are the majority carriers and holes are the minority carriers. A common dopant for n-type silicon is phosphorus or arsenic. In an n-type semiconductor, the Fermi level is greater than that of the intrinsic semiconductor and lies closer to the conduction band than the valence band. [25]

Figure I.5: Band structure of an n-type semiconductor. Dark circles in the conduction band are electrons and light circles in the valence band are holes. The image shows that the electrons are the majority charge carrier.
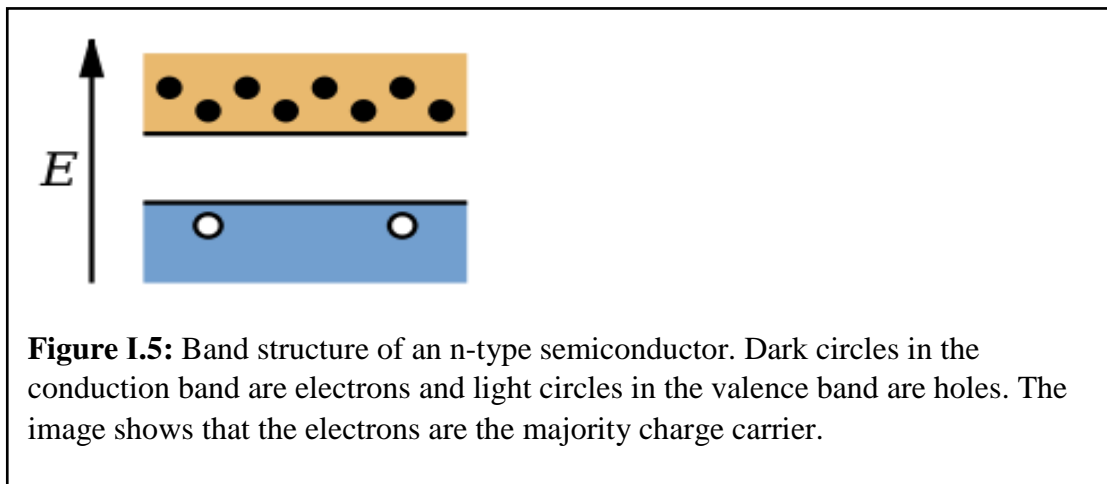
I.4.4.2 P-type semiconductors

P-type semiconductors are created by doping an intrinsic semiconductor with an electron acceptor element during manufacture. The term *p-type* refers to the positive charge of a hole. As opposed to *n-type* semiconductors, *p-type* semiconductors have a larger hole concentration than electron concentration. In *p-type* semiconductors, holes are the majority carriers and electrons are the minority carriers. A common *p-type* dopant for silicon is boron or gallium. For *p-type* semiconductors the Fermi level is below the intrinsic Fermi level and lies closer to the valence band than the conduction band. [26]

Figure:I.6 Band structure of a p-type semiconductor. Dark circles in the conduction band are electrons and light circles in the valence band are holes. The image shows that the holes are the majority charge carrier
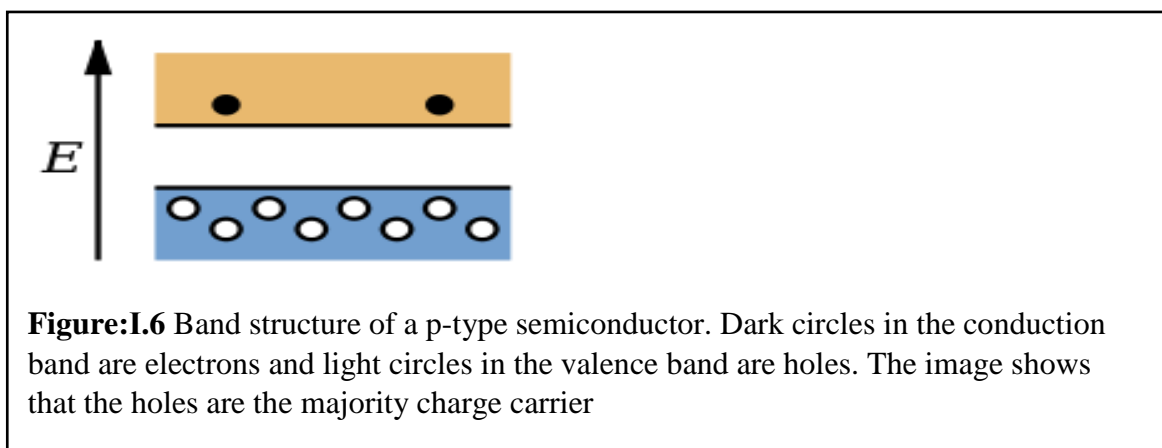
I.4.4.3 P–N Junction

A p–n junction is a boundary or interface between two types of semiconductor materials, p-type and n-type, inside a single crystal of semiconductor. The "p" (positive) side contains an excess of holes, while the "n" (negative) side contains an excess of electrons in the outer shells of the electrically neutral atoms there. This allows electrical current to pass through the junction only in one direction. The p-n junction is created by doping, for example by ion implantation, diffusion of dopants, or by epitaxy (growing a layer of crystal doped with one type of dopant on top of a layer of crystal doped with another type of dopant). If two separate pieces of material were used, this would introduce a grain boundary between the semiconductors that would severely inhibit its utility by scattering the electrons and holes.

p–n junctions are elementary "building blocks" of semiconductor electronic devicessuch as diodes,transistors, solar cells, LEDs, and integrated circuits; they are the active sites where the electronic action of the device takes place. For example, a common type of transistor, the bipolar junction transistor, consists of two p–n junctions in series, in the form n–p–n or p–n–p; while a diode can be made from a single p-n junction. A Schottky junction is a special case of a p–n junction, where metal serves the role of the p-type semiconductor. [27]

Figure:I.7 .A p–n junction. The circuit symbol is shown: the triangle corresponds to the p side
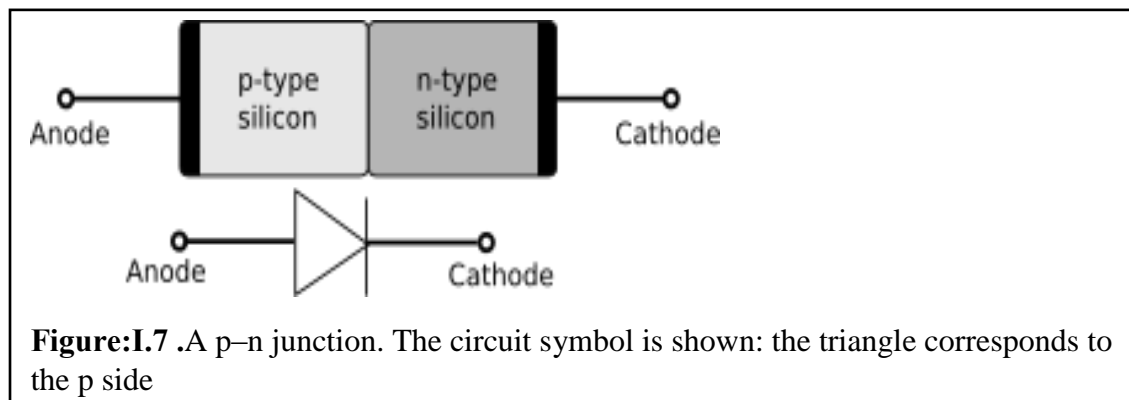
I.4.5 Doping

Doping is a technique used to vary the number of electrons and holes in semiconductors. Doping creates N-type material when semiconductor materials from group IV are doped with group V atoms. P-type materials are created when semiconductor materials from group IV are doped with group III atoms.[28]

N-type materials increase the conductivity of a semiconductor by increasing the number of available electrons; P-type materials increase conductivity by increasing the number of holes present.

n- type :$n_0 = N_D$, $p_0 = \dfrac{n_i{}^2}{N_D}$

p-type :$p_0 = N_A$, $n_0 = \dfrac{n_i{}^2}{N_A}$

where N_D is the concentration of donor atoms and N_A is the concentration of acceptor atoms.

I.4.5 Absorption in Semiconductors

Absorption in semiconductors is a so-called basic lattice absorption, in which one electron is excited out of the valence band into the conduction band, leaving a hole in the valence band. Certain peculiarities of this process should be taken into account.

I.5 solar cells

A solar cell, or photovoltaic cell, is an electrical device that converts the energy of light directly into electricity by the photovoltaic effect, which is a physical and chemical phenomenon[29]. It is a form of photoelectric cell, defined as a device whose electrical characteristics, such as current, voltage, or resistance, vary when exposed to light. Individual solar cell devices can be combined to form modules, otherwise known as solar panels. The common single junction silicon solar cell can produce a maximum open-circuit voltage of approximately 0.5 to 0.6 volts.[30]

I.5.1 The Working Principle of a Solar Cell

Illustrating the absorption of a photon in a semiconductor with bandgap Eg. The photon with energy $E_{ph} = h\nu$ excites an electron from E_i to E_f. At E_i a hole is created. (b) If $E_{ph} > E_G$, a part of the energy is thermalised.

theband gap energyis energy difference,$E_g = E_c - E_v$. If a photon with energy smaller than E_G reaches an ideal semiconductor, it will not be absorbed but will traverse the material without interaction.

FigureI.8 (a) Illustrating the absorption of a photon in a semiconductor with bandgapE_G . The photon with energy $E_{ph} = h\nu$excites an electron from $E_i$to E_f. At E_i a hole is created. (b) If $E_{ph}>E_G$, a part of the energy is thermalised.
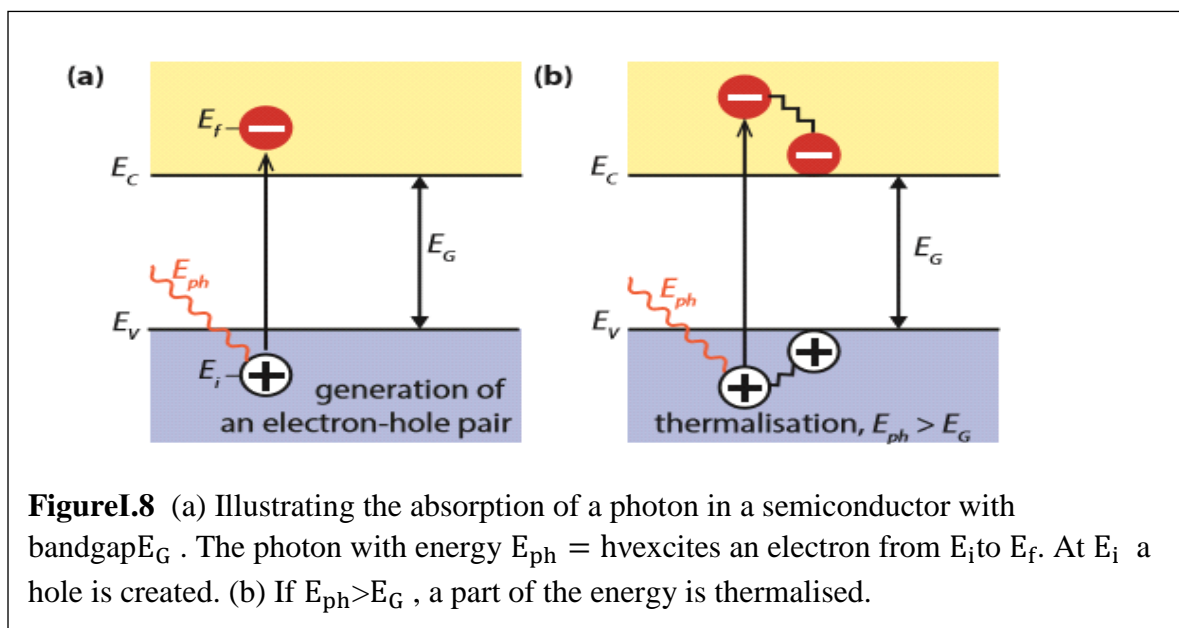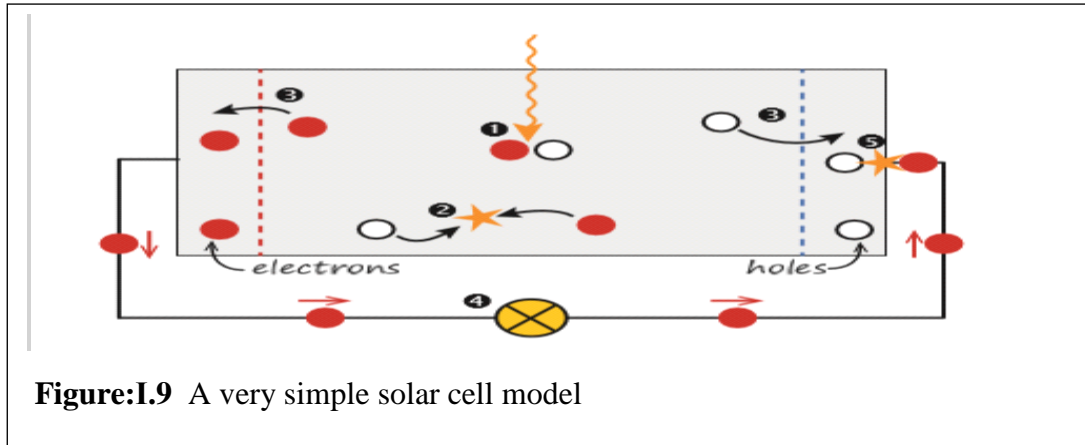
Figure:I.9 A very simple solar cell model

(1)Absorption of a photon leads to the generation of an electron-hole pair.

(2) Usually, the electrons and holes will recombine.

(3)With semipermeable membranes the electrons and the holes can be separated.

(4)The separated electrons can be used to drive an electric circuit.

(5) After the electrons passed through the circuit, they will recombine with holes.

If one wants to use the energy stored in the electron-hole pair for performing work in an external circuit , semipermeable membranes must be present on both sides of the absorber, such that electrons only can flow out through one membrane and holes only can flow out through the other membrane[31] , as illustrated in Fig.(I.9) (3)‚. In most solar cells, these membranes are formed by n- and p-type materials.

A solar cell has to be designed such that the electrons and holes can reach the membranes before they recombine, i.e. the time it requires the charge carriers to reach the membranes must be shorter than their lifetime. This requirement limits the thickness of the absorber.

Finally, the charge carriers are extracted from the solar cells with electrical contacts so that they can perform work in an external circuit Fig.(I.9)(4). The chemical energy of the electron hole pairs is finally converted to electric energy. After the electrons passed through the circuit, they will recombine with holes at a metal-absorber interface, as illustrated in Fig.I.9 (5).

I.5.2 Basic Equations of Semiconductor Device Physics

I.5.2.1 Poisson's Equation

$$-\frac{d^2\varphi}{dx^2} = \frac{dE}{dx} = \frac{Q}{\varepsilon_0\varepsilon} \tag{I.10}$$

$$\frac{dE}{dx} = \frac{q}{\varepsilon_0\varepsilon}(p - n + N_D^+ - N_A^-) \tag{I.11}$$

Where φ is the electrostatic potential, ε_0 is the permittivity of free space and ε is the static relative permittivity of the medium

I.5.2.2 The Current Density Equations

For the electrons

$$I_n = q(n\mu_n E + D_n \frac{dn}{dx}) \tag{I.12}$$

and likewise for the holes

$$I_p = q(p\mu_p E + D_p \frac{dp}{dx}) \tag{I.13}$$

where n and p are electron and hole densities, μ_n and μ_p are the electron and hole mobilities and D_e and D_P are the electron and hole diffusion constants.

I.5.2.3 The Continuity Equations

$$J_n(x) = qD_n \frac{dn(x)}{dx} + q\mu_n n(x)E(x) \tag{I.14}$$

$$J_p(x) = -qD_p \frac{dp(x)}{dx} + q\mu_p p(x)E(x) \tag{I.15}$$

The first terms on the right hand side of Eqs. I.14 and 1.15 are diffusion currents driven by a concentration gradient, and the second terms are drift currents driven by the electric field E

$$0 = \frac{1}{q}\frac{dJ_p(x)}{dx} + G_p(x) - R_p(x) \tag{I.16}$$

$$0 = \mu_p p\frac{dE(x)}{dx} + \mu_p E\frac{dp(x)}{dx} + D_p\frac{d^2p(x)}{dx} + G_p(x) - R_p \tag{I.17}$$

$$0 = \frac{1}{q}\frac{dJ_n(x)}{dx} + G_n(x) - R_n(x) \tag{I.18}$$

$$\mathbf{0} = \mu_n n\frac{dE(x)}{dx} + \mu_n E\frac{dn(x)}{DX} + D_n\frac{d^2n(x)}{dx^2} + G_n(x) - R_n(x) \tag{I.19}$$

where R(x) and areG(x) the position-dependent volume recombination and photogeneration rates, respectively

I.5.3 Device parameters

I.5.3.1 Short circuit current

The short circuit current is the current through the solar cell when the voltage across the solar cell is zero (when the solar cell is short circuited). Usually written as I_{sc} . The short circuit current and the light –generated current are identical.itis the largest current which many be drawn from the solar

Figure:I.10 Short circuit current
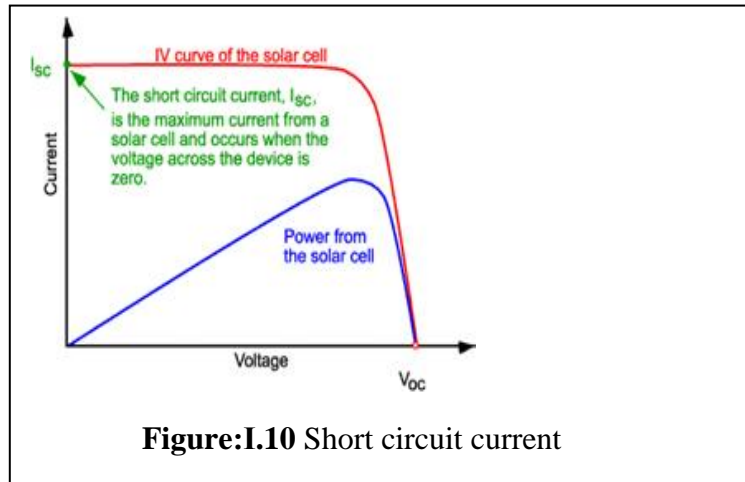
I.5.3.2 Open circuit voltage

The open circuit voltage V_{oc} , is the maximum voltage available from a solar cell, and this occurs at zero current .The open circuit voltage expresses the direct polarization of the resulting cell by polarizing the junction with the light –generated current . The schematic of the open circuit

Voltage on the I-V   curve is in figure   (I.11).

$$I_0(e^{\left(\frac{eV_{oc}}{K_BT}\right)} - 1) - I_{sc} = 0 \tag{I.20}$$

$$V_{oc} = \left(\frac{K_BT}{e}\right) \ln(\frac{I_{sc}}{I_0} - 1) \tag{I.21}$$

Figure:I.11 Open circuit voltage
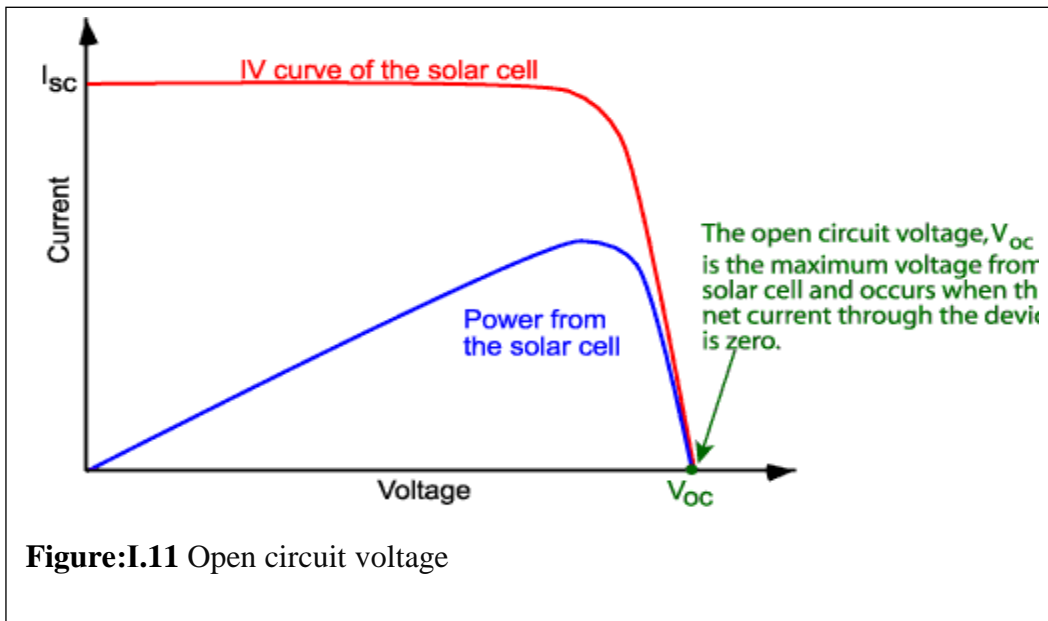
I.5.3.3 The Fill Factor FF

The Fill Factor is the ratio of maximum power P_m to the open-circuit V_{oc} voltage and short-circuits current I_{SC} . It is known by the abbreviation ''FF''. Graphically , the fill factor is measure of the '' squareness '' of the solar cell and is also the area of the largest rectangle which will fit in the IV curve . The FF is illustrated in figure (I.12).

$$FF = \frac{I_m \cdot V_m}{I_{sc} \cdot V_{oc}} = \frac{P_m}{I_{sc} \cdot V_{oc}} \tag{I.22}$$

Figure:I.12 The Fill Factor FF
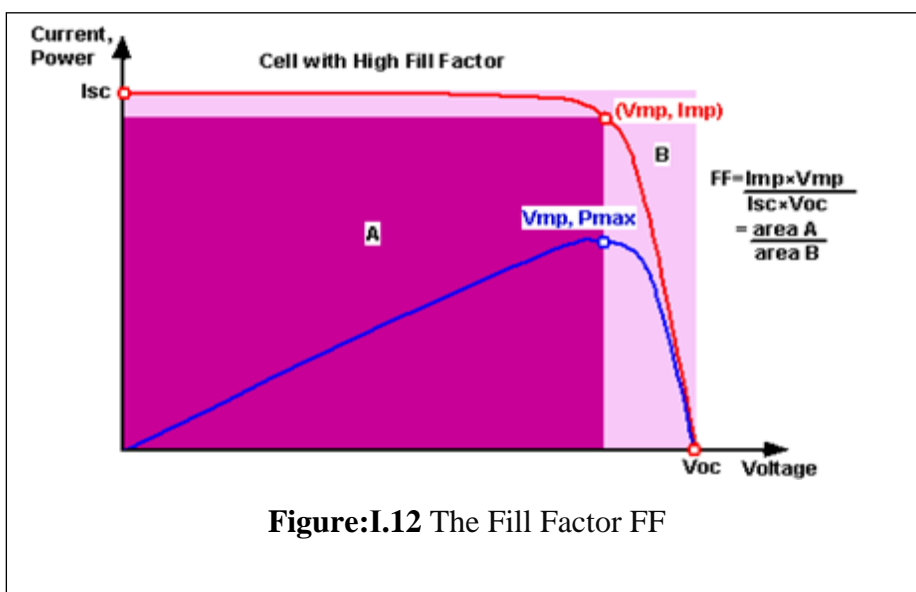
I.5.3.4 Conversion Efficiency

The conversion efficiency n is the most important figure of merit and it is defined as the ratio of the maximum output power to the incident power.

$$n = \frac{P_{out}}{P_{in}} \tag{I.23}$$

I.5.3.5   Quantum Efficiency

By definition , the quantum efficiency QE is the ratio of the number of carriers collected by the solar cell to the number of photons of a given energy incident on the solar cell . It may be given either as a function wavelength or as energy. The quantum efficiency can be I if all photons are absorbed and all minority carriers resulting are collected, in a certain wavelength. It is measured in electrons per photon or amps per watt.

$$QE = \frac{n}{n_{ph}} \tag{I.24}$$

Where n is the number of electrons, and n_{ph} is the number of photons .

I.5.3.6 External quantum Efficiency (EQE)

Which is the ratio of the number of charge carriers collected by the solar cell to the number of photons of a given energy incident on the solar cell from outside.

$$EQE = \frac{\text{electrons·s}^{-1}}{\text{absorbed photons.s}^{-1}} = \frac{\text{current (e)}}{\text{total photon power}} \tag{I.25}$$

I.5.3.7 Internal Quantum Efficiency

It indicates the ratio of the number of charge carriers collected by the solar cell to the number of photons of a given energy that shine on the solar cell from outside and are absorbed by the cell.

$$IQE = \frac{electron·s^{-1}}{absorbed p\square otons·s^{-1}} = \frac{EQE}{1-Reflection} \tag{I.26}$$

I.5.4 The structure of the solar cell

Crystalline solar cells usually consist of several support and link layers, anti-reflective and metal conduction layers.As for non-crystalline solar cells that have a structure that differs from crystalline cells, forexample, in pigment solar cells , it consists of transparent transport glass

(front and back), titanium dioxide, dye, and electrolyte.For amorphous silicon it has the same structure as crystalline silicon cells

Back connection: the metal is distributed over the entire area of the semiconductor with respect to silicon. Usually we use a layer of aluminum and then a layer of copper.

Front conduction: only certain areas are connected where they leave areas for the passage of light. Usually, in silicon we use a mixture of silver, palladium and titanium.

Reflex layer: to reduce reflection and they use ITO, SiO_2 , TiO_2 ,Ta_2O_3 ,SiN_3.

The predicate and joint are made according to the cell used and the materials made of it.

Electrolyte is an electrochemical solution called a medium .

Tincture: it is a light-sensitive, organic, molecular dye called sensitization S.

Clear Conveying Glass: it is a transparent glass with a thin layer of transparent conductive oxide such as ITO, FTO this oxide represent the positive and negative electrodes.

I.5.5 Generation of solar cells

I.5.5.1 First-Generation PV Technolgies: Crystalline Silicon Cells

The earliest commercial silicon traditional solar cells are made from silicon, are currently the most efficient solar cells available for residential use and account for around above 80 % of all the solar panels sold around the world. Silicon solar cells are the most efficient in terms of single cell photovoltaic devices, and silicon is the most abundant element on earth, only second to oxygen. It is a semiconductor material suitable for PV applications, with energy band gap of 1.12eV. Crystalline silicon cells are classified into three main types depending on how the Si wafers are made. The types are based on the type of silicon used, specifically:

-Monocrystalline

- Polycrystalline (Poly c-Si);

-Amorphous.

I.5.5.2 Second-Generation PV Technologies: Thin-Film Solar Cells

Second-generation solar cells are also known as thin-film solar cells because when compared to crystalline silicon based cells they are made from layers only a few micrometers thick. After more than 20 years of R&D, thin-film solar cells are beginning to be deployed in significant quantities. Thin-film solar cells could potentially provide lower cost electricity than c-Si wafer-based solar cells. Thin-film solar cells are comprised of successive thin layers, just 1 to 4 µm thick,such as glass, polymer, or metal. Thin films can be packaged into flexible and lightweight structures, which can be easily integrated into building components (building-integrated PV, BIPV).

There are basically three primary types of thinfilm solar cells that have been commercially developed:

-Amorphoussilicon (a-Si and a-Si/μc-Si);

-Cadmium Telluride (Cd-Te);

-Copper-Indium-Selenide (CIS) and CopperIndium-Gallium-Diselenide (CIGS).

   most solar cells used in calculators and many small electronic devices are made from amorphous silicon cells. Instead of growing silicon crystals as is done in making the two previous types of solar cells, silicon is deposited in a very thin layer on to a backing substrate – such as metal, glass or even plastic. One advantage of using very thin layers of silicon is that the panels can be made flexible. The disadvantage of amorphous panels is that they are much less efficient per unit area (up to 12%) [32].

I.5.5.3 Third- Generation PV Technologies

   Due to high costs of first generation solar cells and toxicity and limited availability of materials for second-generation solar cells, a new generation of solar cells emerged. Currently there is a lot of solar research going on in what is being referred to in the in the industry as Third-generation solar cells. Third generation solar cells are inherently different from the previous two generations because they do not rely on the p-n junction design of the others. This new generation of solar cells are being made from variety of new materials besides silicon, including nanomaterials, silicon wires, solar inks using conventional printing press technologies, organic dyes, and conductive plastics. The goal of course is to improve on the solar cells already commercially available solar energy more efficient over a wider band of solar energy , less expensive and without any toxicity so it can be used by more and more people, and to develop more and different uses. Dye-sensitized solar cells are also frequently calledGrätzel cells named after the developer. DSSCs separate the absorption of photons from the energy generation. Among various solar cells, dye-sensitized solar cells (DSSCs) demonstrate specific advantages over other photovoltaic devices, because of their high efficiency, low cost, simple fabrication procedures, environmental friendliness, transparency, and good plasticity. Though DSSCs perform well under laboratory conditions relative to other solar cells, parameters such as efficiency, lifetime, and cost determine their commercial applications. The major components of conventional DSSCs include a nanocrystalline semiconductor oxide, a dye sensitizer, a redox electrolyte, and a counter electrode (CE).[33,34] Recently, extensive studies of the individual components of DSSCs have been performed to reduce production costs and to achieve high cell performance.

First Generaton	.Monocrystalline(Mono c-Si) .Polycrystalline(Poly c-Si),and .AorphouseSiliconCells
Second Generation	.Amorphoussilicon(a-Si and a-Si/μc-Si) ; .Cadmium Telluride(Cd-Te) ; and .Copper-Indium-Selenide(CIS) and Copper-Indium-Gallium-
Third Generation	.Dye sensitised (DSSC) .Perovskite (cell) .Organic (OPV)

Figure:I.13 Classification of PV cells
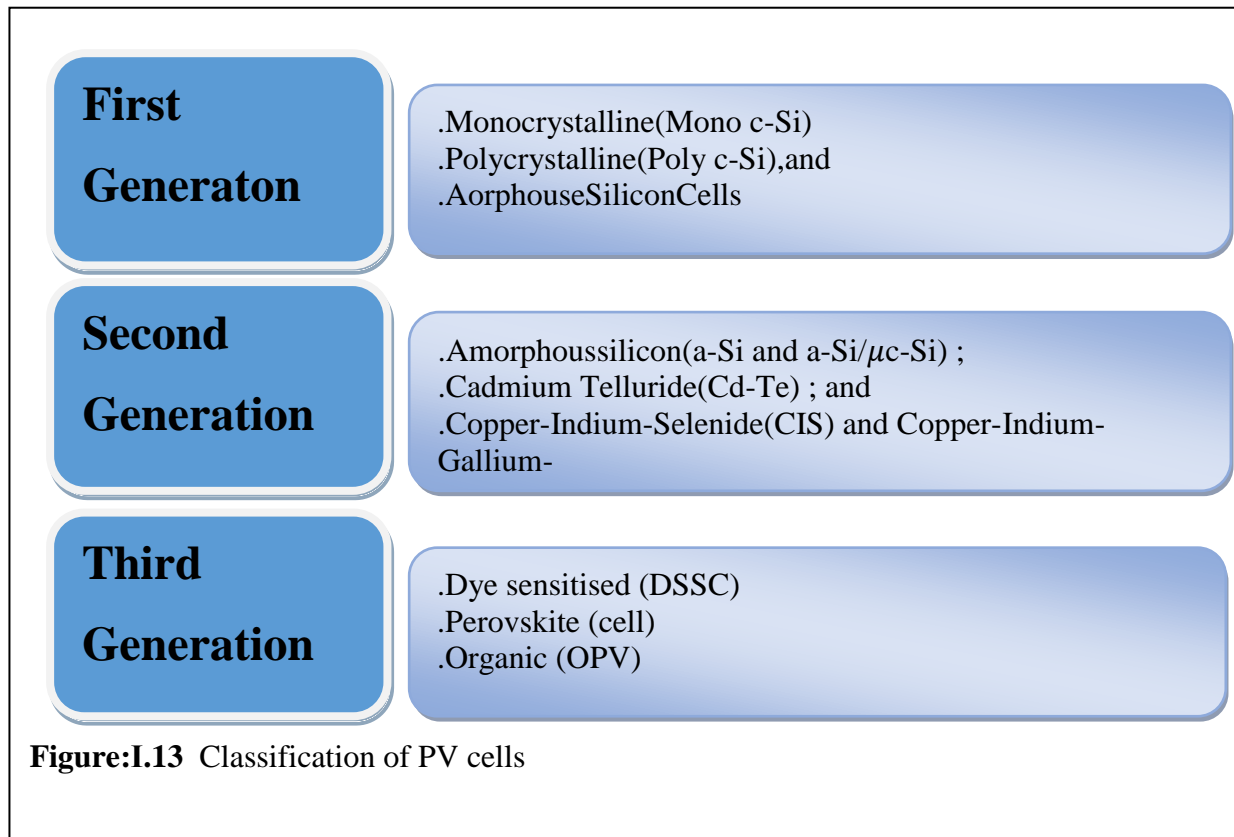
TableI.2 A table that Efficiency some solar cell

Classification	Efficiency (%)	Area (cm2)	Voc (v)	Jsc (mA/m2)	Fill Factor(%)
silicon					
Si(crystalline cell)	25.6±0.5	143.7	0.740	41.8	82.7
Si(multicrystallin cell)	21.3±0.4	242.74	0.6678	39.8	80.0
III-V cells					
GaAs(thin film cell)	28.8±0.9	0.9927	1.122	29.68	86.5
CIGS(cell)	21.0±0.6	0.9927	0.757	35.70	77.6
CZTSSe(cell)	9.8±0.2	1.115	0.5073	31.95	60.2
Si(amorphous cell)	10.2±0.3	1.001	0.896	16.36	69.8
Perovskite					
Perovskite(cell)	19.7±0.6	0.9917	1.104	24.67	72.3
Organic					
Organic(cell)	11.2±0.3	0.992	0.780	19.3	74.2
Multijunction					
InGaP/GaAs/InGaAs	37.9±1.2	1.047	3.065	14.27	86.7
a-Si/nc-Si(thin film cell)	12.7±0.4	1.000	1.342	13.45	70.2
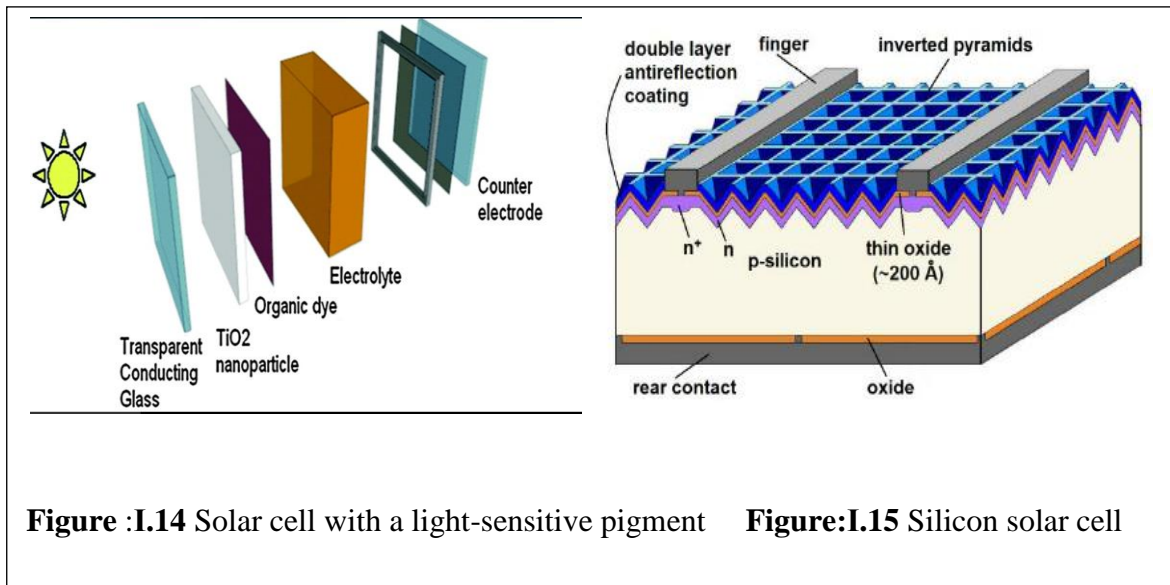
Figure :I.14 Solar cell with a light-sensitive pigment   **Figure:I.15** Silicon solar cell
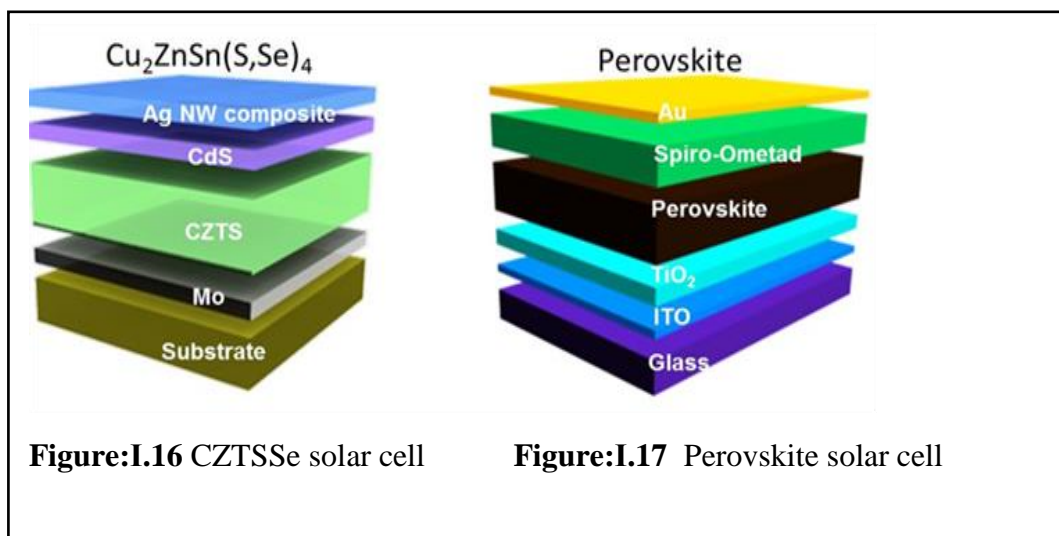
Figure:I.16 CZTSSe solar cell   **Figure:I.17** Perovskite solar cell

I.5.6 Multijunction Solar Cells

Jackson proposed the multijunction concept in 1955 [35], whereby the solar spectrum is absorbed selectively by solar cells of different band-gaps, thereby preserving a greater fraction of the free-energy received from high energy photons. Figure 1.18 shows how the efficiency rises 67% under one sun, it is clear that much of the gain to be made through this approach can be realised with only a couple of junctions. The key requirement is to partition the solar spectrum at the appropriate point and direct the sunlight to semiconductors with different band-gapenergies chosen to match the bandwidth of sunlight incident upon them.

Figure:I.18 Efficiency for a series constrained multijunction solar cell under AM1.5G ill umination.(Data extracted with permission from Brown, 2002. [36] Copyright C, Elsevier.)
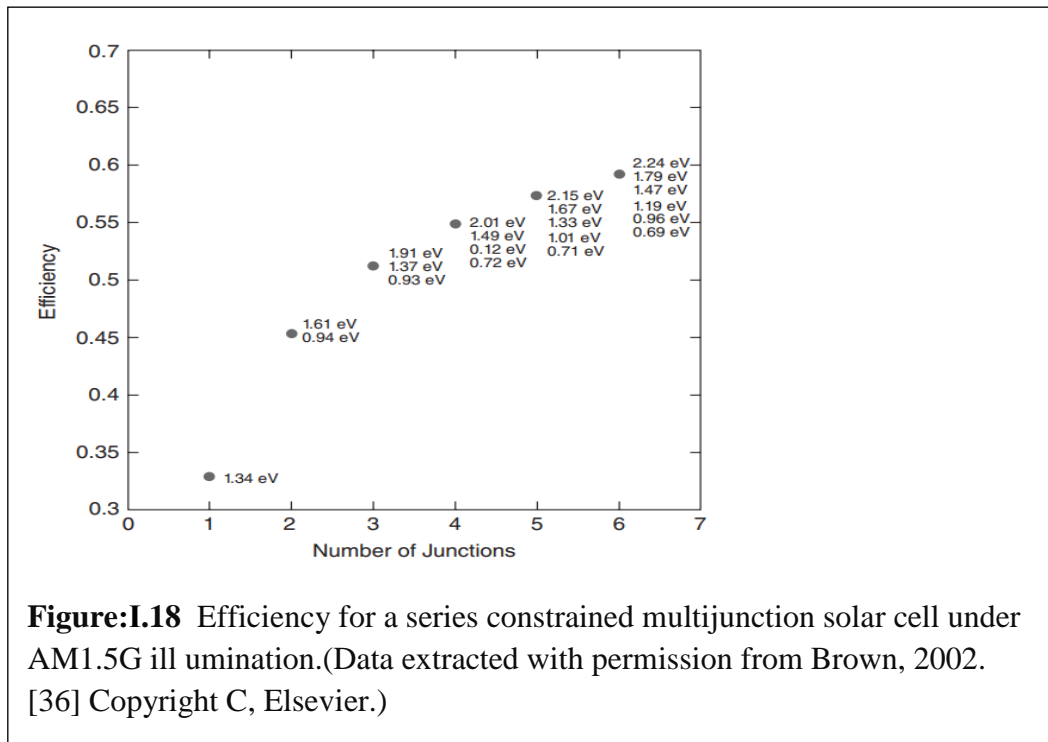
In order for a solar cell to work, the energy from incoming photons must have enough energy to give electrons in the valence band sufficient energy to move to the conduction band.Electrons are able to conduct to the conduction band without difficulty but are often conducted so far beyond, or 'overshoot', the conduction band that a large portion of the energy is lost to heat the in the crystal lattice as the electron moves to a lower energy state at the bottom of the conduction band. If the energy of incoming photons is smaller than the band gap, electrons are not given sufficient energy to move from the lower energy valence band to the higher energy conduction band, and the incoming photons are not absorbed by the solar cell thus passing through the material. This leaves a challenge to efficiently move electrons to the conduction band and lose as little energy as possible to the lattice from overshooting. The solar spectrum incorporates photons of different energy based on different wavelengths, so a single p-n junction solar cell will only have limited range for conversion efficiency where electrons move just beyond the conduction band and lattice heat loss is limited. The solution to this efficiency challenge is to use multiple p-n junctions stacked on top of each other with differing band gap values such that together they are able to absorb a wider range of the solar spectrum. This idea is referred to as Multijunction Solar Cells [37]. An example of the increased absorption can be seen in Figure (I.19)
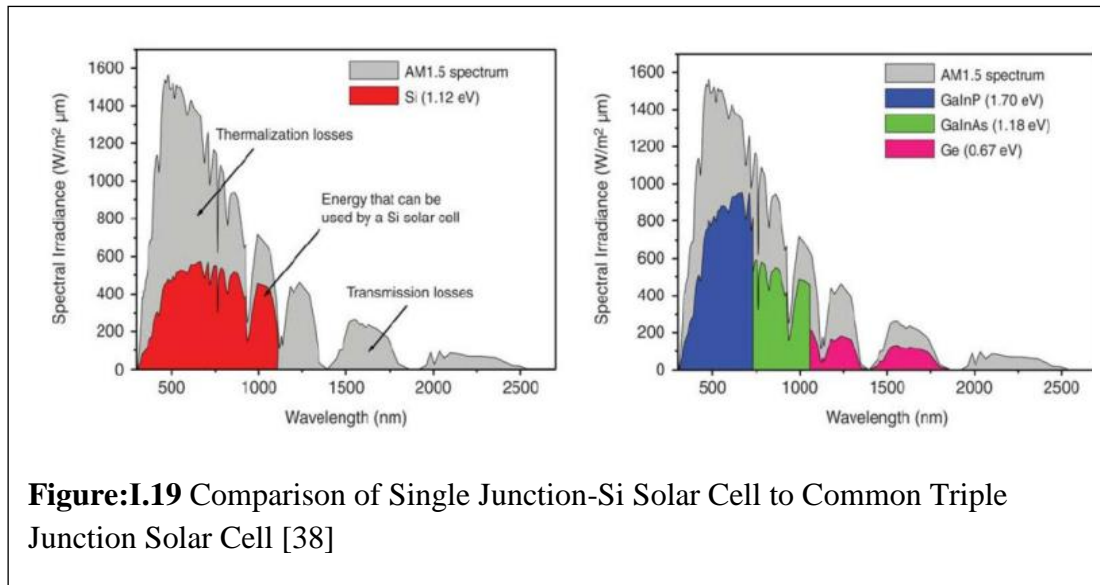
Figure:I.19 Comparison of Single Junction-Si Solar Cell to Common Triple Junction Solar Cell [38]

Multijunction or "Tandem" solar cells use a combination of different semiconductor materials to form junctions to optimize the conversion of photons into electricity. Multijunction cells were first studied in the 1960s and projected theoretical maximums in efficiency were between 38.2% and 51% depending on manufacturing technique [39]. Advancements in semiconductor technology have elevated the theoretical maximum efficiency of multijunction cells to 86.8% from those first projected values in the 1960s. Progress in the development of multijunction efficiency has shown promising results [38]. From some of the initial demonstrations in the 1980s of 16% to the current record of 43.7% set by Solar Junction in the middle of 2011 by using Concentrated PVs with a dilute nitride cell architecture, it is expected that within the coming years concentrated multijunctions for commercial use will reach efficiencies of 50%.[40]

I .5.6.1 Monolithic Multijunction Solar Cells

The Integration of all the components for a multijunction solar cell into one monolithic structure places some constraints upon the multijunction solar cell design. In general, the highestquality semiconductor junctions are achieved using lattice-matched semiconductor material. However,since the subcells are connected together in series internally, the current passing the solar cell will be limited by the junction producing the lowest current. It is therefore important to engineer subcells producing similar current at maximum power and this can be difficult to achieve using only lattice-matched materials, so a number of monolithic lattice-mismatched (or metamorphic) multijunction solar cells have been attempted where the lattice parameter is graded from one semiconductor junction to another. The typical band structure for a double-junction solar cell is shown in Figure I.20, showing the physical stacking of semiconductor layers and the band structure. Many of the components from the single junction solar cell are present, notably the presence of a window layer and backsurface field. The interconnection of the junctions is critically important in a monolithic cell and is achieved using a tunnel junction. Typically, tunnel junctions are formed by growing a heavily doped n++, layer

adjacent to a heavily doped p++ layer, thereby bringing the conduction band of the n++ semiconductor to almost overlap energetically with the valence band of the p++ semiconductor. In principle, the remaining barrier is sufficiently thin to enable a substantial tunnelling current to pass, but simulations show that the high tunnel currents measured experimentally are likely to be enhanced through trap-assisted tunelling[41, 42]. In practice, tunnel junctions can be difficult to achieve. Firstly the junction must be transparent, meaning relatively high-bandgap semiconductors must be used, increasing the doping density required to achieve the same peak tunnel current [43]. Secondly, actually achieving very abrupt p++/n++ layers and preventing dopant diffusion during the remainder of the epitaxial growth is also challenging. One important means for preventing dopant diffusion has been the use high-bandgap materials (typically AlGaAs or AlInGaP) that act as diffusion barriers around the tunnel junction [44–45] as well as serving as useful window/BSF layers; for clarity these barriers are not shown in Figure (I.20).
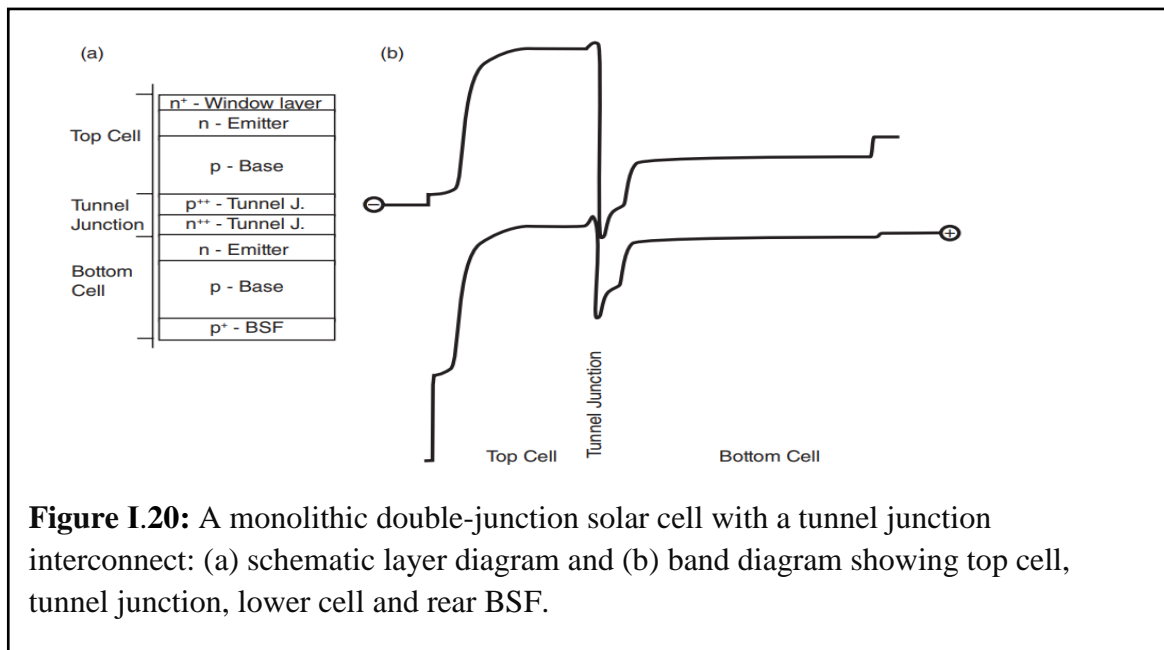
Figure I.20: A monolithic double-junction solar cell with a tunnel junction interconnect: (a) schematic layer diagram and (b) band diagram showing top cell, tunnel junction, lower cell and rear BSF.

I.6 Conclusion

In this chapter, we provided the basics of some concepts about solar radiation, and also presented a brief history of solar cells, semiconductors, and in the end we talked about how solar cells work and her generations.

In the next chapter, we will introduce the basic properties of silicon ,CZTSSe and the Simulation program.

Chapter II :

MATERIALS PROPERTIES AND SIMULATION SOFTWARE

II.1 introduction

In this chapter, we will first look at a brief definition of the materials used in our work, such as silicon and CZTSSe.

Secondly, we will learn about the program used in this research to achieve the synthesis of cells, the first generation silicon cell and the second generation cell CZTSSe.

II.2 Materials

II.2.1 Silicon

Silicon material is one of the most important materials for technology applications because it is the backbone of the microelectronics industry as well as the most biocompatible material. It is the least toxic material, promising to be a green technology. It was Canham who first showed in 1990 that visible red photoluminescence light (PL) can come out of silicon wafer crystals at room temperature when electrochemically etched [46]. A magic family of silicon nanoparticles are produced in Nayfeh's lab at the University of Illinois from bulk silicon by a special patented electrochemically dispersion process. The family consists of highly luminescent stable particles of 1, 1.7, 2.2, 2.9 nm in diameter [47]. Unlike bulk silicon, a spectacularly dull material, the silicon nanoparticle family is spectacularly efficient at emitting light in RGB colors, covering the blue, green, yellow, and red part of the spectrum respectively when exposed to dark ultraviolet radiation.

Figure:II.1 Silicon (Si) 14 Metalloid

II.2.1.1 Production

Silicon of 96–99% purity is made by reducing quartzite or sand with highly pure coke. The reduction is carried out in an electric arc furnace, with an excess of SiO_2 used to stop silicon carbide (SiC) from accumulating:[48]

$SiO_2 + 2\,C \rightarrow Si + 2\,CO$

$2\,SiC + SiO_2 \rightarrow 3\,Si + 2\,CO$
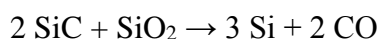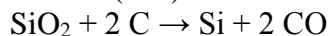
This reaction, known as carbo thermal reduction of silicon dioxide, usually is conducted in the presence of scrap iron with low amounts of phosphorus and sulfur, producing ferro silicon.[48] Ferro silicon, an iron-silicon alloy that contains varying ratios of elemental silicon and iron, accounts for about 80% of the world's production of elemental silicon, with China, the leading supplier of elemental silicon, providing 4.6 million tonnes (or 2/3 of world output) of silicon, most of it in the form of ferro silicon. It is followed by Russia (610,000 t), Norway (330,000 t), Brazil (240,000 t), and the United States (170,000 t).[49] Ferrosilicon is primarily used by the iron and steel industry (see below) with primary use as alloying addition in iron or steel and for de-oxidation of steel in integrated steel plants.[48] Another reaction, sometimes used, is alumino thermal reduction of silicon dioxide, as follows.[50]

$3\ SiO_2 + 4\ Al \rightarrow 3\ Si + 2\ Al_2O_3$
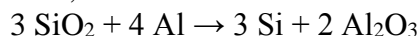
Leaching powdered 96–97% pure silicon with water results in ~98.5% pure silicon, which is used in the chemical industry. However, even greater purity is needed for semiconductor applications, and this is produced from the reduction of tetrachloro silane or trichloro silane. The former is made by chlorinating scrap silicon and the latter is a byproduct of silicone production. These compounds are volatile and hence can be purified by repeated fractional distillation, followed by reduction to elemental silicon with very pure zinc metal as the reducing agent. The spongy pieces of silicon thus produced are melted and then grown to form cylindrical single crystals, before being purified by zone refining. Other routes use the thermal decomposition of silane or tetraiodo silane. Another process used is the reduction of sodium hexa fluoro silicate, a common waste product of the phosphate fertilizer industry, by metallic sodium: this is highly exothermic and hence requires no outside fuel source. Hyperfine silicon is made at a higher purity than almost every other material: transistor production requires impurity levels in silicon crystals less than 1 part per 10^{10}, and in special cases impurity levels below 1 part per 10^{12} are needed and attained.[48]

II.2.1.2 Crystal structure

Silicon crystallises in a giant covalent structure at standard conditions, specifically in a diamond cubic lattice. It thus has a high melting point of 1414 °C, as a lot of energy is required to break the strong covalent bonds and melt the solid.

Naturally occurring silicon is composed of three stable isotopes, ^{28}Si (92.23%), ^{29}Si (4.67%), and ^{30}Si (3.10%).[51]

Figure:II.2 crystal structure of Si
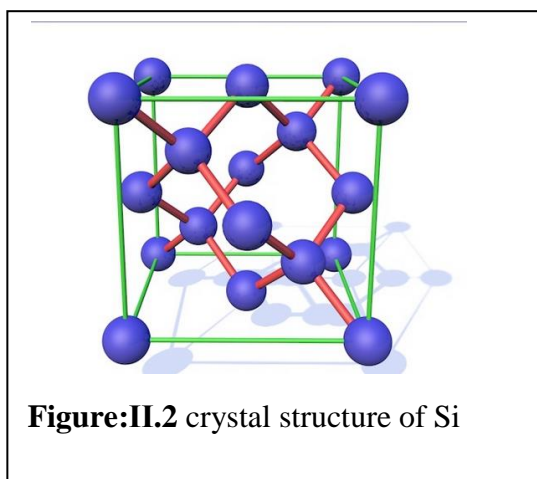
II.2.1.3 Electrical structure

At standard temperature and pressure, silicon is a shiny semiconductor with a bluish-grey metallic lustre; as typical for semiconductors, its resistivity drops as temperature rises. This arises because silicon has a small energy gap (band gap) between its highest occupied energy levels (the valence band) and the lowest unoccupied ones (the conduction band). The Fermi level is about halfway between the valence and conduction bands and is the energy at which a state is as likely to be occupied by an electron as not. Hence pure silicon is effectively an insulator at room temperature. However, doping silicon with a pnictogen such as phosphorus, arsenic, or antimony introduces one extra electron per dopant and these may then be excited into the conduction band either thermally or photo lytically, creating an n-type semiconductor. Similarly, doping silicon with a group13element such as boron, aluminium, or gallium results in the introduction of acceptor levels that trap electrons that may be excited from the filled valence band, creating a p-type semiconductor.[52]

II.2.1.4 Other properties

P (Pa)	1	10	100	1 k	10 k	100 k
at T (K)	1908	2102	2339	2636	3021	3537

Iso-tope	Abun-dance
^{28}Si	92.2%
^{29}Si	4.7%
^{30}Si	3.1%
^{31}Si	trace
^{32}Si	Trace

	solid
Melting point	1687 K (1414 °C, 2577 °F)
Boiling point	3538 K (3265 °C, 5909 °F)
Density (near r.t.)	2.3290 g/cm^3
when liquid (at m.p.)	2.57 g/cm^3
Heat of fusion	50.21 kJ/mol
Heat of vaporization	383 kJ/mol
Molarheatcapacity	19.789 J/(mol·K)

Crystal structure	face-centered diamond-cubic
Speed of sound thin rod	8433 m/s (at 20 °C)
Thermal expansion	2.6 μm/(m·K) (at 25 °C)
Thermal conductivity	149 W/(m·K)
Electricalresistivity	2.3×10^3 Ω·m (at 20 °C)
Band gap	1.12 eV (at 300 K)
Magneticordering	diamagnetic
Magneticsusceptibility	$-3.9 \cdot 10^{-6}$ cm^3/mol (298 K)
Young'smodulus	130–188 GPa
Shearmodulus	51–80 GPa
Bulkmodulus	97.6 GPa
Poisson ratio	0.064–0.28
Mohshardness	6.5
CAS Number	**7440-21-3**
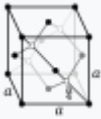
II.2.1.5 Chemistry and compounds

Crystalline bulk silicon is rather inert, but becomes more reactive at high temperatures. Like its neighbouraluminium, silicon forms a thin, continuous surface layer of silicon dioxide (SiO_2) that protects the metal from oxidation. Thus silicon does not measurably react with the air below 900 °C, but formation of the vitreous dioxide rapidly increases between 950 °C and 1160 °C and when 1400 °C is reached, atmospheric nitrogen also reacts to give the nitrides SiN and Si_3N_4. Silicon reacts with gaseous sulfur at 600 °C and gaseous phosphorus at 1000 °C. This oxide layer nevertheless does not prevent reaction with the halogens; fluorine attacks silicon vigorously at room temperature, chlorine does so at about 300 °C, and bromine and iodine at about 500 °C. Silicon does not react with most aqueous acids, but is oxidised and fluorinated by a mixture of concentrated nitric acid and hydrofluoric acid; it readily dissolves in hot aqueous

alkali to form silicates. At high temperatures, silicon also reacts with alkyl halides; this reaction may be catalysed by copper to directly synthesiseorganosilicon chlorides as precursors to silicone polymers. Upon melting, silicon becomes extremely reactive, alloying with most metals to form silicides, and reducing most metal oxides because the heat of formation of silicon dioxide is so large. As a result, containers for liquid silicon must be made of refractory, unreactive materials such as zirconium dioxide or group 4, 5, and 6 borides.[52]

II.2.1.6 The Structure of Ahigh Efficiency Solar Cell

The base material is mono crystalline, float zone pulled and p-doped (approximately $1.5 \times 10^{16} cm^{-3}$), with a resistivity of approximately 1 Ωm. The base thickness is approximately 200 µm, primarily due to technological manufacturing and handling processes. The front surface facing the light is textured, preferably with inverted pyramids The front surface, apart from the grid structure, is coated with a thermally grown layer of silicon dioxide for passivation. The emitter is two stage and has a surface doping concentration of approximately 1 $x10^{19} cm^{-3}$ and a penetration depth of 0.5-1 µm , the surface concentration is approximately 1 x $10^{20} cm^{-3}$ and the penetration depth approximately 2-3 µm under the metal of the grid structure.

The back surface of the cell is coated with a thermally grown SiO_2, layer for passivation except for the point contacts (approximately 1%-2% of the total area).

The local p^+-doped BSF has a surface concentration of $>10^{20} cm^{-3}$ and a penetration depth of 2-3 µm. The SiO_2, passivation has a thickness of approximately 100 nm to achieve a high antireflection effect on the emitter side (light entry). The back surface contact has reflective characteristics and consists, for example, of vapour-deposited aluminium. For a cell of dimensions 2x2 cm² the grid Jingers have a width of approximately 15 µm and a thickness of around 8 µm (tapering away from the busbar).

The busbar has a width of approximately 150 µm, and the contact connection is located in the middle of the busbar.

By implementing these measures it is possible to increase the efficiency of monocrystalline solar cells in the laboratory under AM1.5 to 23%-24%, very close to the theoretical efficiency [53]-[54].

A further increase in efficiency can be achieved in crystalline silicon by using thinner cells of approximately 10-30 µm. However, this requires excellent passivation of the crystal surface and very good 'optical confinement'.

Figure:II.3 Basic schematic of a silicon solar cell.The top layer is referred to as the emitter and the bulk material is referred to as the base
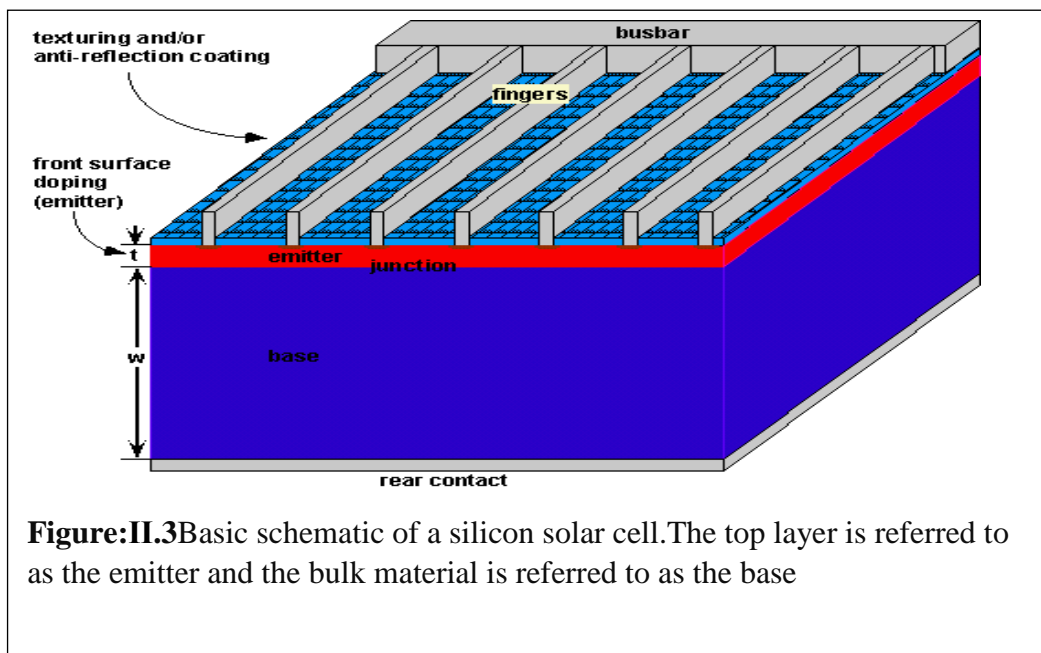
II.2.1.7 Optical Losses

Optical losses chiefly effect the power from a solar cell by lowering the short-circuit current. Optical losses consist of light which could have generated an electron-hole pair, but does not, because the light is reflected from the front surface, or because it is not absorbed in the solar cell.

There are a number of ways to reduce the optical losses:

- Top contact coverage of the cell surface can be minimised (although this may result in increased series resistance).

- Anti-reflection coatings can be used on the top surface of the cell.

- Reflection can be reduced by surface texturing.

- The solar cell can be made thicker to increase absorption (although light that is absorbed more than a diffusion length from the junction has a low collection probability and will not contribute to the short circuit current).

- The optical path length in the solar cell may be increased by a combination of surface texturing and light trapping.

- A further reduction in reflectivity is achieved through a *double layer anti-reflection* coating (DLARC). Popular DLARC coatings are zinc sulfide (ZnS) with magnesium flouride (MgF) or layers of silicon nitride with varying refractive index.

- Lambertian back reflector is a special type of rear reflector which randomizes the direction of the reflected light. High reflection off the rear cell surface reduces absorption in the rear cell contacts or transmission from the rear, allowing the light to bounce back into the cell for possible absorption.xpensive for most commercial solar cells[55].

II.2.2 CZTSSe

CdTe and Cu(In,Ga)Se$_2$ (CIGSe) solar cells have achieved remarkable efficiencies exceeding 20%. However, elements such as indium and tellurium are rare, and cadmium is quite toxic, which may limit the implementation of these devices at the terawatt scale. In recent years, Cu$_2$ZnSnS$_4$ (CZTS), Cu$_2$ZnSnSe$_4$ (CZTSe), and Cu$_2$ZnSn(S,Se)$_4$ (CZTSSe) have emerged as replacement materials for thin-film PV due to promising optoelectronic properties and the use of nontoxic, earth-abundant elements.

II.2.2.1 History of CZTSSe

CZTS was first investigated as a solar cell material in 1988 at Shinshu University in Japan. The researchers deposited thin films of CZTS using sputtering and measured p-type conductivity, a direct band gap of 1.45 eV, and absorption coefficients exceeding 10^4 cm^{-1} in the visible range.[56] They reported a solar cell the next year with a V$_{oc}$ of 0.165 V, though the J$_{sc}$ was very low. In 1996, the first solar cells based on CZTS and CZTSe absorbers using cadmium sulfide/zinc oxide window layers were reported with efficiencies exceeding 0.6%.[57] Further research continued over the next decade, with improvements to processing conditions and window layers, resulting in efficiencies nearing 7%.[58] Around this time, research into solution processing of CZTSSe cells began.[59]In 2013, IBM's Watson Research Center was able to push the efficiency of a lab-scale solar cell to 12.6% using a hydrazine-based solution process; this stands as the world record for a CZTSSe-based solar cell toda.

II.2.2.2 The Crystal Structures of CZTSSe

CZTS may crystallize in a zincblende-derived structure similar to other semiconductor materials such as silicon and CIGSe. Conceptually, this kesterite CZTS cell is formed by substituting half of the In/Ga sites in CIGSe with Zn and the other half with Sn. However, CZTS can have two other forms. The stannite structure has the same tetragonal coordination, but different symmetry due to alternate placement of cations in the crystal lattice. The wurtzite-derived structure is a hexagonal close-packed array. All three have the nominal Cu$_2$ZnSnS$_4$ stoichiometry, though the kesterite structure is used most often in solar

cells.[60] Note that the CZTSSe and CZTSe compounds adopt analogous structures to those of CZTS

Figure:II.4 crystal structures of semiconductor materials.
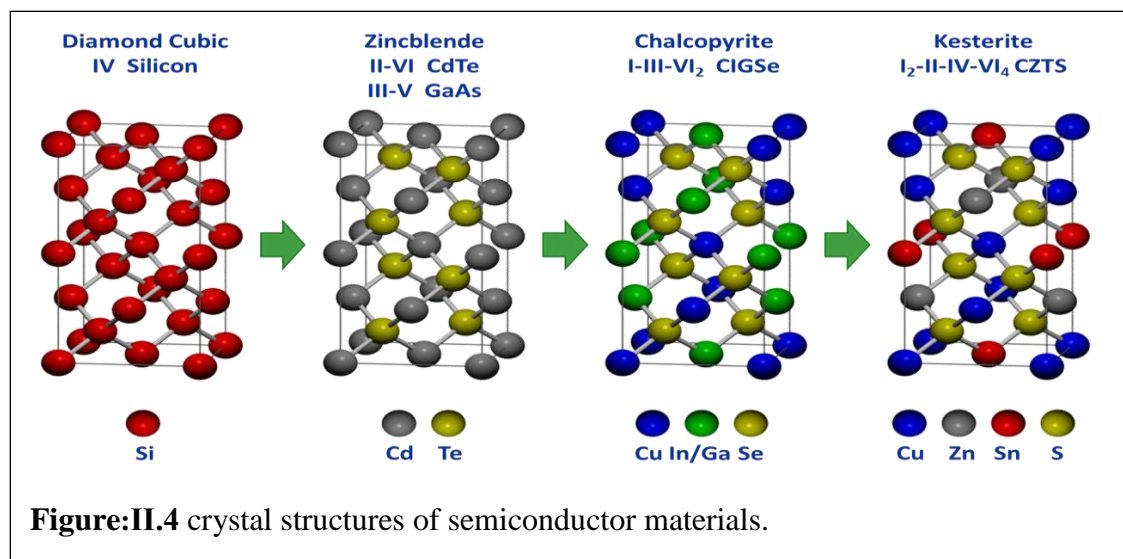
Table:II.1 Selection of CZTSSe solar cell devices with conversion efficiency≥6%.[61]

	Institute	Material	Method	T (C)	η (%)	Voc (mV)	Jsc (mA/ cm2)	FF
Vacuum	Stanford University	CZTSSe	Co-sputtering	580	9.3			
	IMEC	CZTSe	DC sputtering	460	9.2	416	37.6	58.7
	NREL	CZTSe	Co-evaporation	500	9.15	377	37.4	64.9
	IBM	CZTS	Evaporation	570	8.4	661	19.5	65.8
	Angst. Solar Center	CZTS	Co-sputtering	560	7.9	667	19.6	60.0
	Luxembourg	CZTSe	Co-evaporation	500	7.5	356	35.4	60.0
	University	CZTS	Co-sputtering	580	6.8	610	17.9	62.0
	Nagaoka Nat. Col	CZTSe	Co-evaporation	500	6.4	330	31.0	63.1
	Delaware University							
Non-vacuum	IBM	CZTSSe	Spin-coating solution+ particl	540	11.1	460	34.5	69.8
	Purdue University	CZTGeS Se	Knife-coating: CZTGeS NPs	500	8.4	464	28.1	62.0
	WA University	CZTSSe	Spin-coating: solution		8.3	440	31.1	60.0
	IBM	CZTS	ED	550-590	7.3	567	22.0	58.1

35

Table II.2 Technological status of a selection of companies in the CZTSSefield[61].

Company	Material	Method	T(c)	η (%)	Voc(Mv)	Jsc (mA/cm2)	FF (%)
SolarFrontier	CZTSSe	Sputtering		10.8	502	33.5	64.0
AQT Solar	CZTSSe	co-sputtering	580	9.3			
							64.9
DuPont	CZTSSe	Spincoating: NPs	560	8.5	4.51	29.0	
Crystalsol	CZTSSe	Monograins		8.4	7.8	16.83	70.9
Toyota	CZTS	Sputtering	580	8.5			

II.2.2.3 Electronic Structure

Calculation of the electronic band structure of CZTS reveals a direct bandgap at the gamma point of the Brillouin zone. While standard DFT calculations at the level of the local density approximation (LDA) or generalized gradient approximation (GGA) grossly underestimate the bandgaps of semiconductors , calculations using hybrid functionals mixed with Hartree-Fock exchange (e.g., HSE[62]) or at the level of many-body perturbation theory (e.g., GW [63]) converge to results around 1.5 eV, which is in good agreement with optical absorption measurements on high quality samples. The prediction of quantitative bandgaps for new materials remains one of the major challenges in computational materials science.[64–65] The magnitude of the bandgap of CZTS can be understood according to the chemical nature of the valence and conduction band states, and in particular, the low binding energy of the filled Cu 3d valence band. The natural band alignments, calculated with reference to the energy difference of deep atomic-like core states across a material heterojunction,[66] are plotted in Figure II.5for a range of common solar cell materials. For all Cu based chalcogenides, including the quaternary and ternary compounds, the valence band maximum (VBM) is an antibonding state of the anion p and Cu d orbitals.[67] The valence p level of S is lower in energy than Se, thus the VBM of the sulfides is lower than that of the selenides; e.g., the VBM is 0.52 eV lower for ZnS than ZnSe,[65] but the difference is reduced by anion p–Cu d overlap (p-d hybridization) in Cu based chalcogenides,because the hybridization is stronger in the shorter Cu–S bondand pushes the antibonding VBM level of the sulfide up relative to that of the selenide. As a result, the valence band offset between the sulphides and selendies is less than 0.2 eV. In contrast, the lower

conduction band is controlled by the metal s states, and for CZTS this is predominately the Sn 5s orbital.

Following the phenomenological doping limit rules of semiconductors,[69–70] the high valence band level should result in good *p*-type conductivity for all Cu(I)-based compounds
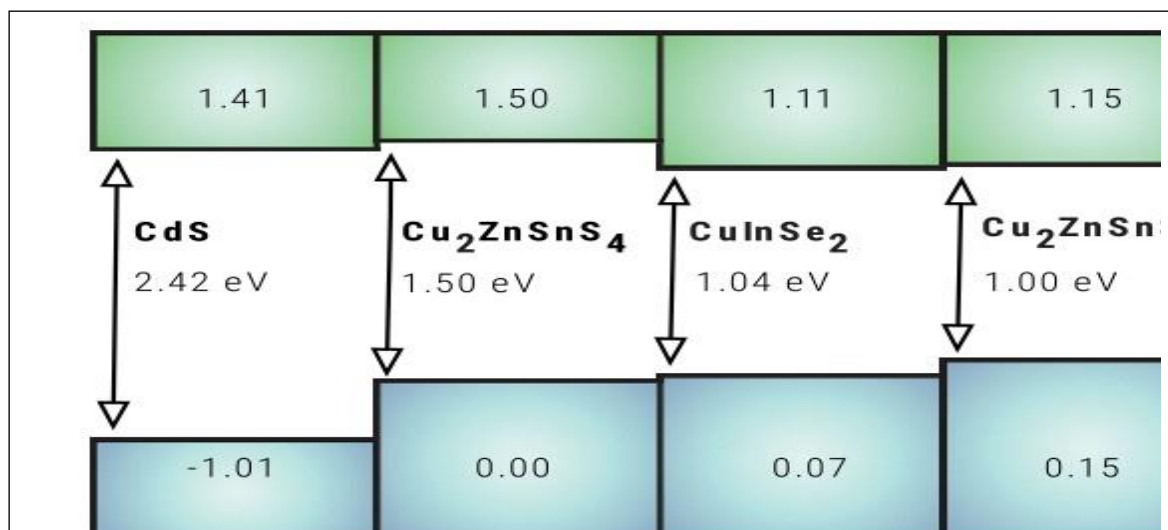
Figure:II.5 The calculated band alignment between CdS, Cu2ZnSnS4,Cu2ZnSnSe4 and CuInSe2 (adapted from Ref. [68]). CdS is a commonly used *n*-type window layer in thin-fi lm solar cells

II.2.2.4ElectricalPropertiesofCu₂ZnSn(S₁₋ₓSeₓ)4 ThinFilms

The $Cu_2ZnSn(S_{1-X}Se_X)_4$ films always exhibit p-type conductivity irrespective of composition ratios that is governed by Cu_{Zn} defects. The defects had lower formation energy. The Cu_{Zn} is more stable among Zn_{Cu} and Zn_{Sn} defects. The paired $(V_{Cu} + Zn_{Cu})$, $(Cu_{Zn} + Zn_{Cu})$, and $(Zn_{Sn} + Sn_{Zn})$ defect levels are fairly formed in the Cu-poor and Zn-rich samples. In fact, the Sn-rich films show very low resistivities [71]. Those passivate deep trap levels and reduce non radiative recombinations [72]. Virtually, the Cu_{Zn} is the dominant acceptor in the CZTS thin films due to lower formation energy and lies above the valence band by 0.1 eV whereas V_{Cu} is the majority acceptor in the Cu-based chalcopyrite semiconductors and locates above the valence band by 0.02 eV. The defect complex $[Cu_{Zn} + Zn_{Cu}]$ is the dominant one in the CZTS system. More importantly, the conduction band shifts toward down side in the band gap when Se is alloyed with S in the $Cu_2ZnSn(S_{1-X}Se_X)_4$ and very low effect in the valence band indicating that the miscibility of anions in the system is quite well [73]. The reason to choose lower Cu/(Zn + Sn) ratio in the range of 0.9-9.8 and Zn/Sn ratio of 1.10 for the fabrication of CZTS thin film solar

cells is that the lower Cu composition may create more copper vacancies while higher Zn concentration may block formation of deeper acceptor level such as antisites Zn_{Cu} [74]. As expected, the resistivity of CZTS films decreases from 3.07 10^{-1} to 3.43 3 $10^{-3}\Omega$-cm and carrier concentration increases from 1.03 10^{19} to 0.83 10^{21} cm^{-3} by increasing Cu composition from 22.4 to 23.1% but the reported range is in narrow window [75]. Therefore, thorough investigation is definitely needed to determine quality of CZTS layers. In another occasion, the resistivity of CZTS films decreases with increasing Cu/(Sn 1 Zn) ratio from 0.64 to 1.17 and also increases with increasing Zn/Sn ratio from 0.73 to 1.42.

II.2.2.5 Point Defect

The calculated ionization levels of point defects in the band-gap of Cu2ZnSnS4, which can be derived from Figure.II.4. It is important to note that the dominant defect CuZn has an acceptor level 0.12 eV above valence band, deeper than that of V_{Cu}(0.02 eV above VBM). The shallow level of V_{Cu} is common in Cu-based Chalcopyrites like CuInSe$_2$ and CuGaSe$_2$ [76]. Low temperature photo luminescence measurements of CZTS identified two shallow acceptor states (10 and 30 meV above the VBM), which could be attributed to two symmetry inequivalent (Cu) vacancy sites. The deep level of the dominant antisite defect is negative for CZTS solar cell efficiency, as it will decrease the open-circuit voltage.

After reference [77], due to the higher number of constituent atoms compared to binary or ternary compounds, CZTSSe has a wider range of possible defects depending on its growth conditions and variations from stoichiometry. Most of them are antisites, vacancies, or interstitials: they can be located shallow or deep in the band-gap, and their concentration depends on their own formation energy [76]. In particular, shallow level defects can influence the minority and majority carrier concentrations thus the conductivity, whereas deep level defects may act as recombination centers for photo generated electron-hole pairs.

Figure:II.4 The ionization levels of intrinsic defects in the band-gap of Cu2ZnSnS4
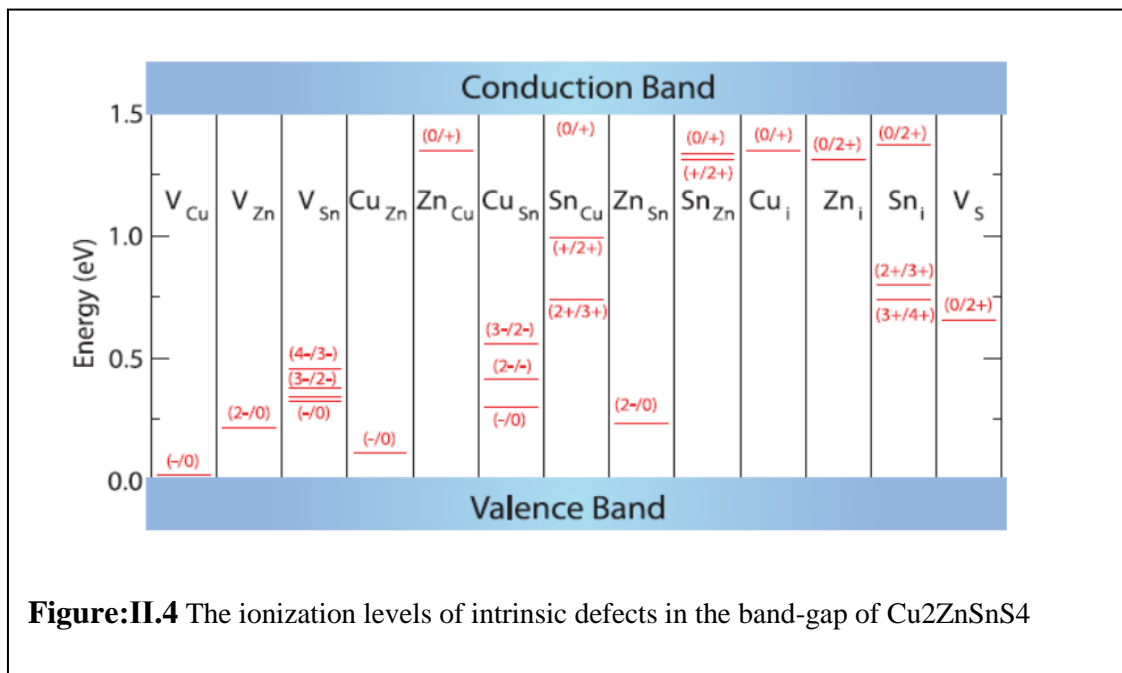
II.2.2.6 Optical properties

The pre-factor of absorption coefficient for the CZTSSe thin film is large enough

($>10^4$ cm^-1) [78,79]. In other word the absorber of just micron thickness is able to absorb sunlight sufficiently, and without any damaging effects on photocurrents. As shown in Figure (II.5).

Figure:II.5: Absorption coefficients $\alpha(\omega)$ as a function of photon energy $\hbar\omega$ for CZTS and of CZTSe from ref [76]
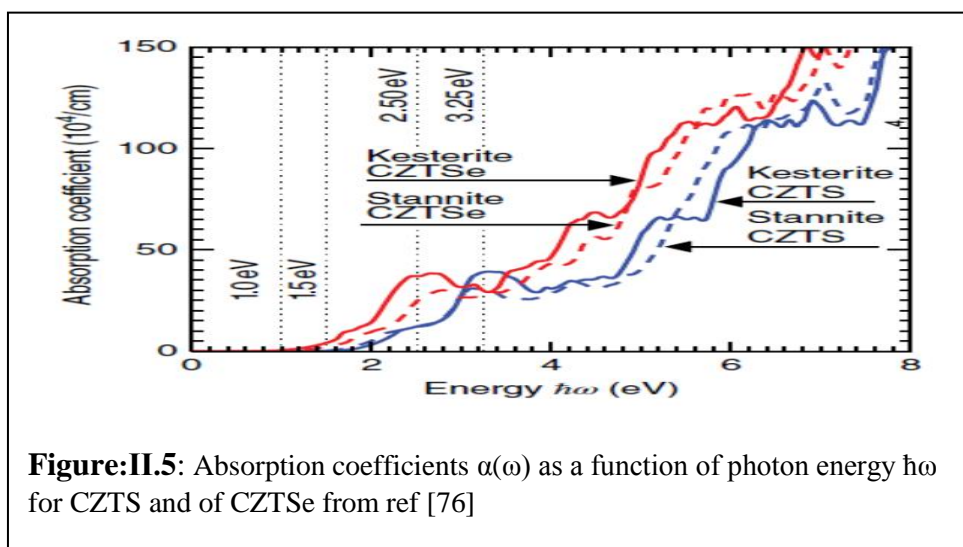
II.2.2.7 CZTSSe Limitations and Future Research Directions

CZTSSe is an inherently challenging material to work with due to its complexity. Forming a phase-pure material is difficult, as its thermodynamic stability window is quite narrow; additionally, Sn-compounds are volatile, and CZTS breaks down at high temperatures. Many secondary phases (particularly Cu_2SnS_3 and ZnS) may coexist in the absence of carefully controlled reaction conditions.[80] Additionally, the stannite and kesterite phases have similar formation energies, so it is likely that a mixture of both can form during synthesis. To complicate matters further, it is difficult to distinguish between these unwanted phases through traditional characterization techniques such as X-ray diffraction.

Crystal structure defects can form quite easily in CZTS. One of the most common defects is an antisite defect – Cu cations can occupy Zn sites and vice versa due to their similar ionic radii. These defects are partially compensated by targeting a Cu-poor, Zn-rich composition during materials synthesis. However, these defects are not eliminated completely and can give rise to band tail states – essentially, these are trap states that arise due to electrostatic potential fluctuations in the material. These states lower the V_{oc} considerably and severely limit the cell's efficiency.[81-82]

Current research is focused primarily on understanding and mitigating the defects within the CZTSSe crystal structure. One potential method is to replace either the Cu or Zn with another atom of a significantly different size (e.g. Cu with Ag or Zn with Ba) to prevent formation of antisite defects, though this could change other material properties such as the conductivity type or crystal structure.[83-84] Another critical area of research focuses on optimizing the solar cell structure, particularly through use of alternative n-type layers that may have energy bands that align more favorably with CZTS.[85]

II.2.2.8 Thin Film Solar Cells $Cu_2ZnSn(S_{1-x}Se_x)_4$

Figure:II.6 Typical architecture of a CZTSSe based solar cell.
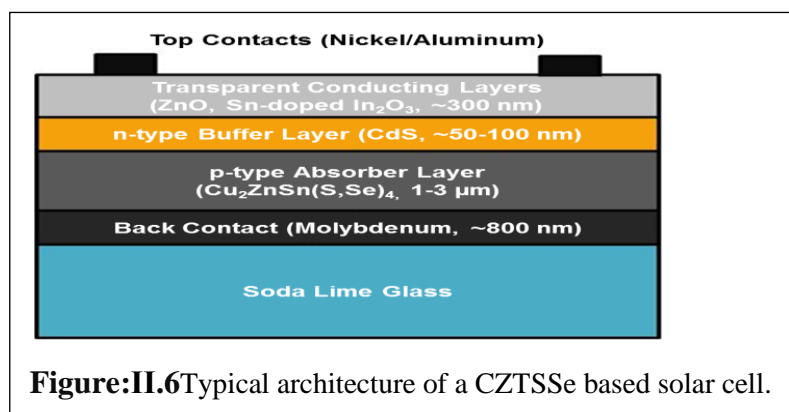
The CZTS nanocrystals ($Cu_{2.12}$ $Zn_{0.84}$ $Sn_{1.06}$ S_4 , Eg = 1.5 eV) made by hot injection process method are converted into CZTSSe (S 5-6%) thin film by selenizing at two different temperatures of 450 and 500 C 0.12 cm^2 area glass/Mo/CZTSSe/CdS (50 nm)/i-ZnO(50 nm)/ITO (250 nm) cells exhibit efficiencies of 0.73 and 0.8% for selenization temperatures of 450 and 500C for 20 min respectively. The low efficiency could be due to Cu-rich in the samples [86]. Directly, the CZTSSe absorber layers grown by spin coating are employed in the thin solar cells, which exhibit reasonably higher efficiencies. The $Cu_{1.8}$ $Zn_{1.2}$ $Sn_{1.06}$ $(S_{0.19}$ $Se_{0.81})_{3.95}$ film by spin coating, 50 nm CdS by CBD, 50 nm ZnO and 250 nm ITO by RF sputtering are successively deposited. The Ni and Al are sequentially deposited for electrodes using mask. The glass/Mo/CZTSSe/CdS/ZnO/ITO/NiAl cells show efficiency of 4.1%. The Zn/Sn ratio increases while converting precursor into device quality absorber layer in the annealing process due to loss of Sn [72]. In fact, the Cu_2S-S (1.2 M) and SnSe-Se are separately dissolved in hydrazine. The Zn powder is added to latter in order to form $ZnSe(N_2H_4)$ and extra S/Se is added to Cu or Sn/Zn chalcogenide solutions. Finally, the mixed solution contains Cu/(Zn + Sn) = 0.8 and Zn/Sn = 1.22. The concentration of solution is diluted to 0.2 M from 0.4 M by adding water. The CZTSSe is successively spin coated onto glass/Mo for six consecutive times at 800 rpm and annealed the layer at 540C under inertic atmosphere of nitrogen. The NiAl grids and MgF2 antireflection coatings are successively coated onto 0.45 cm2 areaglass/Mo/$Cu_2ZnSn(S,Se)_4$/CdS/ZnO cells, which show efficiencies of 9.6 and 8.1% for the absorber made by undiluted and diluted hydrazine [87]. Similarly, 1.2 M Cu_2S-S solution is developed by dissolving Cu_2S and S in hydrazine and similarly, 0.57 M SnSe-Se and Zn solution is made by dissolving SnSe,Se, and Zn in hydrazine. But excess Se is added to the solution. Both solutions are mixed to form slurry of Cu_2S-S + SnSe-Se + $ZnSe(N_2H_4)$ with composition ratios of Cu/(Zn + Sn) =0.8, Zn/Sn = 1.22, and S/(S + Se) = 0.03 in the final film. In order to obtain 2-2.5 μm thick CZTSSe thin-film, five successive depositions are consistently carried out by spin coating at 800 rpm. The precursor CZTSSe layer is vigorously heated at 540C on hot plate without providing sulfur but excess Se is taken in the precursor solution. After annealing CZTSSe samples, which turn out to be low quantity S sample due to loss of sulfur and the MoSe2 phase forms about 300 nm thick at backside of the layer. The CdS by CBD, ZnO and ITO by RF sputtering are sequentially grown onto the CZTSe samples. Ni/Al grids and 110 nm MgF2 are grown by electron beam evaporation. 300 nm thick MoSe2 is observed between Mo

and CZTSSe sample. The CZTSSe film used in the solar cells shows band gap of 1.04 eV and the cells with an area of 0.447 cm^2 show the highest record efficiency of 10.1%.

II.3 Commonly used simulation software

In this part, we will present a selection of currently available numerical simulation tools for thin-film solar cells. Many other numerical simulation programs than those discussed here are in use:

-Quokka2,

-Quokka3

-PC1D

-I2E(+PC1D)

-SCAPS

-ADEPT

-OPV Lab

-Setfos

-QS Cell

-SARAH(IBC)

-wxAMPS

-Gpvdm

II.3.1 AMPS

This program, called AMPS(Analysis of Microelectronic and Photonic Structures), numerically solves the three governing semiconductor device equations (the Poisson equation and the electron and hole continuity equations) without making any a-priori assumptions about the mechanisms controlling transport in these devices. With this general and exact numerical treatment, AMPS may be used to examine a variety of device structures that include

Homo junction and hetero junction p-n and p-i-n, solar cells and detectors;
homo junction and hetero junction p-n, p-i-n, n-i-n, and p-i-p microelectronic structures;
multi-junction solar cell structures;
multi-junction microelectronic structures;
compositionally-graded detector and solar cell structures;

compositionally-graded microelectronic structures;

novel device microelectronic, photovoltaic, and opto-electronic structures;

Schottky barrier devices with optional back layers.

II.3.2 An Overview of How AMPS Works

In briefly overviewing our methods of modeling microelectronic and opto-electronic devices, we first note that the physics of device transport can be captured in three governing equations: Poisson's equation, the continuity equation for free holes, and the continuity equation for free electrons. Determining transport characteristics then becomes a task of solving these three coupled non-linear differential equations, each of which has two associated boundary conditions. In AMPS, these three coupled equations, along with the appropriate boundary conditions, are solved simultaneously to obtain a set of three unknown state variables at each point in the device: the electrostatic potential, the hole quasi-Fermi level, and the electron quasi-Fermi level. From these three state variables, the carrier concentrations, fields, currents, etc. can then be computed. To determine these state variables, the method of finite differences and the Newton-Raphson technique are incorporated by the computer. In AMPS, the one-dimensional device being analyzed is divided into segments by a mesh of grid points, the number of which the user decides. The three sets of unknowns are then solved for each particular grid point. We note that AMPS allows the mesh to have variable grid spacing at the discretion of the user. As noted, once these three state variables are obtained as a function of x, the band edges, electric field, trapped charge, carrier populations, current densities, recombination profiles, and any other transport information may be obtained.

II.3.3 Examples of AMPS Output

II.3.3.1 An Example— a Triple Junction Solar Cell

Figure II.7. gives the illuminated current-voltage characteristic and the cell performance values obtained from AMPS simulation of an a triple p-i-n solar cell. The density of states used to model the a-Si:H materials consists of exponential tail states and midgap states. Figure (II.8). shows the band diagram of this complicated cell in thermodynamic equilibrium. Figure (II.9) shows the electron and hole lifetime at open circuit voltage. This example illustrates AMPS usefulness in determining the transport mechanisms controlling cell performance and in optimizing cell design. In addition, this final example also highlights the versatility of AMPS by demonstrating its ability to model complicated structures with many layers of different materials.

Figure: II.7 Illuminated current-voltage characteristic and cell performance values for this triple junction solar cell.

Figure:II.8 Band diagram of this triple junction in thermodynamic equilibrium.
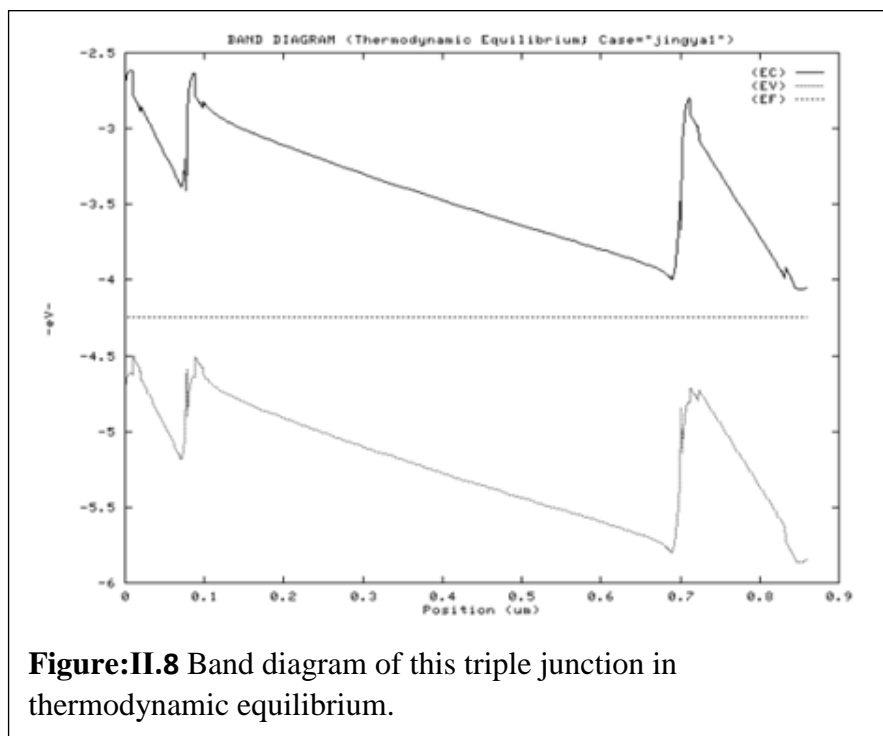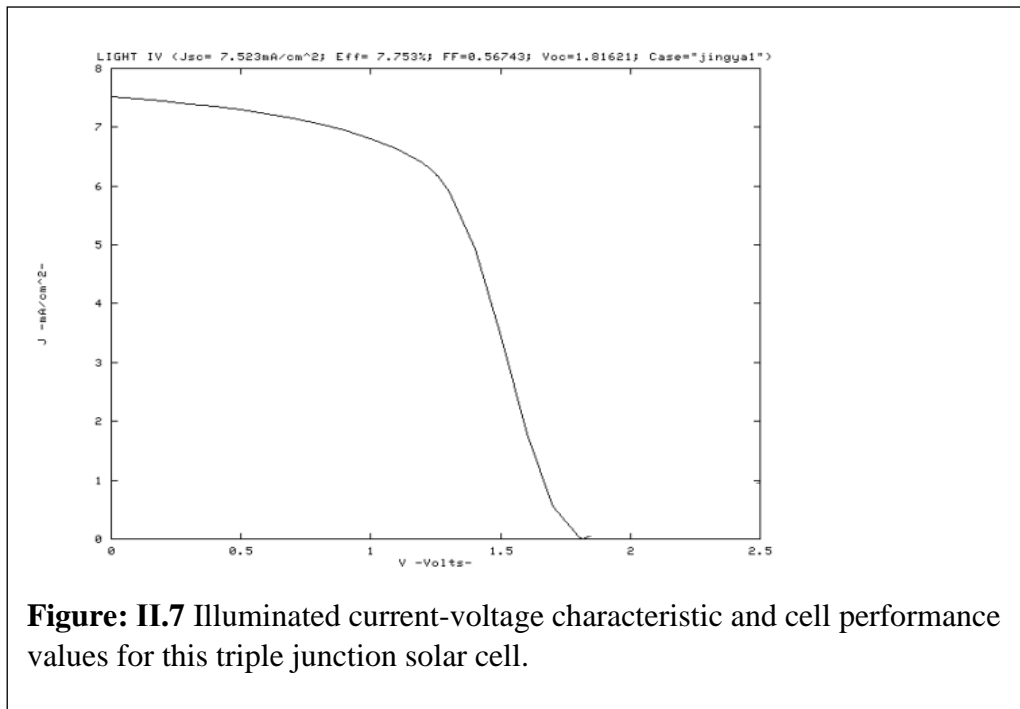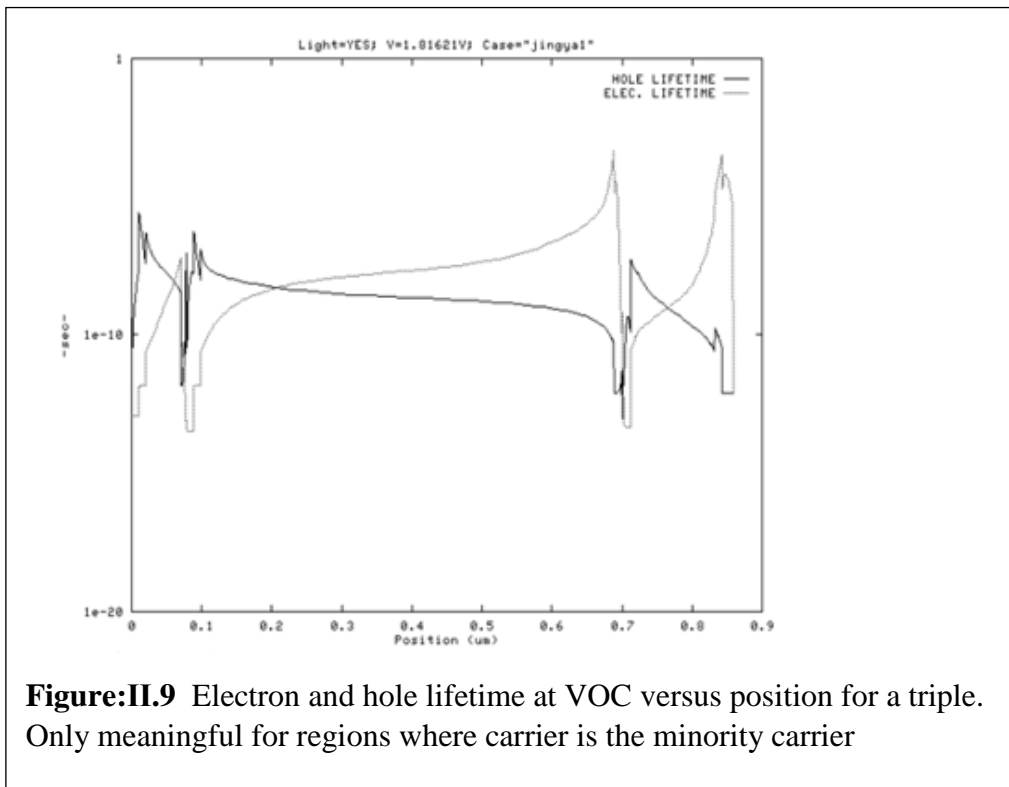
Figure:II.9 Electron and hole lifetime at VOC versus position for a triple. Only meaningful for regions where carrier is the minority carrier

II.3.4wxAMPS

The wxAMPS program is a newly developed solar cell simulation software based on the original AMPS (Analysis of Microelectronic and Photonic Structures) code.[88] The graphical user interface (GUI) of wxAMPS is designed with a cross-platform C++ library, wxWidgets, and allows quick data entry as well as enhanced visualization of results for comparison and analysis. The main physical principles are derived from AMPS [89] and in addition two different tunneling models, intra-band tunneling [90] and trapassisted tunneling [91], are incorporated to the program. The algorithm of wxAMPShas been modified to combine the Newton and Gummel methods, which improves convergence and stability. The effects of series and shunt resistance unrelated to the main diode are also added.

A database-oriented WIKI [92] has been set up for sharing the simulation files of devices and helping users find and discuss the parameters used in solar cell simulations. wxAMPS is a good tool to simulate various kinds and structures of solar cells, which can be made from crystalline and amorphous Si material, as well as CdTe and CIGS thin films, and other materials. Tandem structured solar cells can also be simulated through using the trap-assisted tunneling model in

which carrier motilities are enhanced as functions of electric fields. The latest runnable version can be obtained at the WIKI website.

II.3.5 Updated Features

II.3.5. 1 Interface

The main user interface Figure II.10 is almost the same as the version described previously [88] with the exception of a "Settings" section under the Run button, allowing users to switch the tunneling models and adjust numerical parameters. In the "Settings" dialog box, users can set up upper limit of iteration times, the convergence precision and the clamping range that is the maximum variables change in one iteration. The variables variation is clamped in order to avoid the overestimation generated by the Newton method.
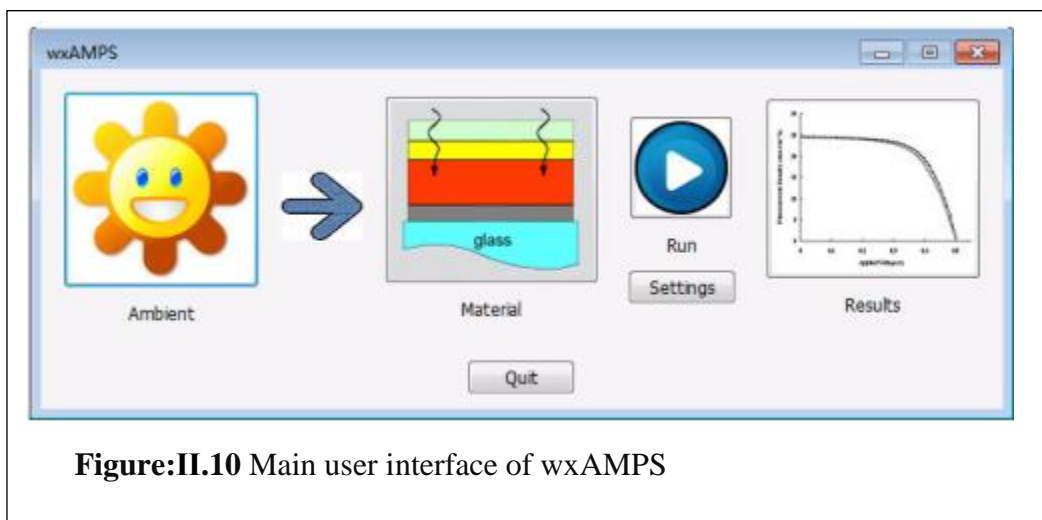
Figure:II.10 Main user interface of wxAMPS

Another improvement is in the ambient dialog box where the bias voltages of interest can be loaded from a use rcustomized text file. The ambient conditions configured previously by the user are cached automatically to help reduce the time spent tweaking the simulation environment. Among these settings, smaller voltage steps and clamping ranges can help improve the convergence property for a specific model, but at a cost of longer calculation time. Two additional slide bars have been added to the results dialog box in order to allow users to modify the values of the series and shunt resistances (Figure II.11). Upon adjustment of the slide bars, a new current-voltage curve is calculated and displayed and new device parameters are obtained. The revised results and the new curve are updated simultaneously when changing the slide bars of the shunt and series resistances.
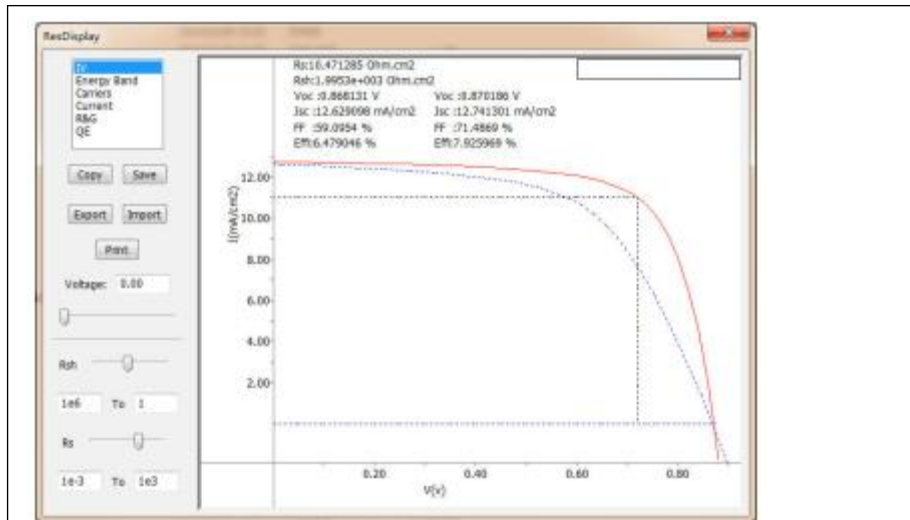
Figure:II.11 Display dialog box for simulation results and analysis

II.3.5.2 Algorithm Modifications

The Gummel method was used in our previous version of wxAMPS to solve the intra-band tunneling current model. Its range of convergence is broad, and it works well on solar cells with low densities of defect states, such as CIGS and CdTe solar cells. However, it encounters difficulty when treating solar cells with high recombination rates, like amorphous Si solar cells. This leads to heavy coupling of the three basic semiconductor equations (Poisson's equation and the continuity equations for electrons and holes), which causes divergence issues. The Newton method is able to solve the strong coupling situation, but makes it difficult to add the intra-band tunneling current into the model for the complicated Jacobian matrix [88], and proper initial values are also important to the convergence.

To solve these mentioned problems, a new algorithm combining the Newton and Gummel methods has been developed. At first, the variables (local vacuum levels and quasi-Fermi levels for electrons and holes) are initialized through a few Gummel iteration steps. Second, a solution is found by using the Newton method in which the drift diffusion model is used but the intra-band tunneling effect is not considered. The solution obtained in the second step is then used as input for the final calculation, employing the Gummel method to add the effects of intraband tunneling current. The trap-assisted tunneling model can be implemented in the Newton method, so the first two steps are enough to achieve the solutions for this model.

II.3.6 Simulation Comparison

II.3.6.1 Performance

The Gummel iterations in the first step of the algorithmn provide more stability for the convergence of the program. Because of the better-initialized guess, wxAMPS works in some cases where AMPS fails with floating number exceptions. Additionally, users will not lose all their information if the simulation does not converge at a certain bias voltage. In the current version, the values calculated during the each simulation step are cached so as to be accessible to the user. The convergence speed is mostly determined by the performance of the third step. In the case of low recombination rates, the Gummel method converges fast and wxAMPS consumes less time than AMPS does. In the case of high recombination rates, the Gummel method may need more iterations to attain the model results when the intra-band tunneling current is added. However, in the trap-assisted model the third step is not required, which makes the calculation much faster.

II.3.6.2 Results

To compare the simulation differences between these models, a baseline CIGS solar cell [93] was simulated.

To study the thermionic emission limit to the current and understand the difference sbetter, the band spike between the CdS and CIGS layers was artificially changed. This was implemented by modifying the electron affinity of the CdS layer. It was found that when the band spike is smaller than the one in the baseline device, the results become much closer. However, when the band spike is 0.3 eV higher than in the baseline case, the differences of the current-voltage curves become obvious Figure II.12.
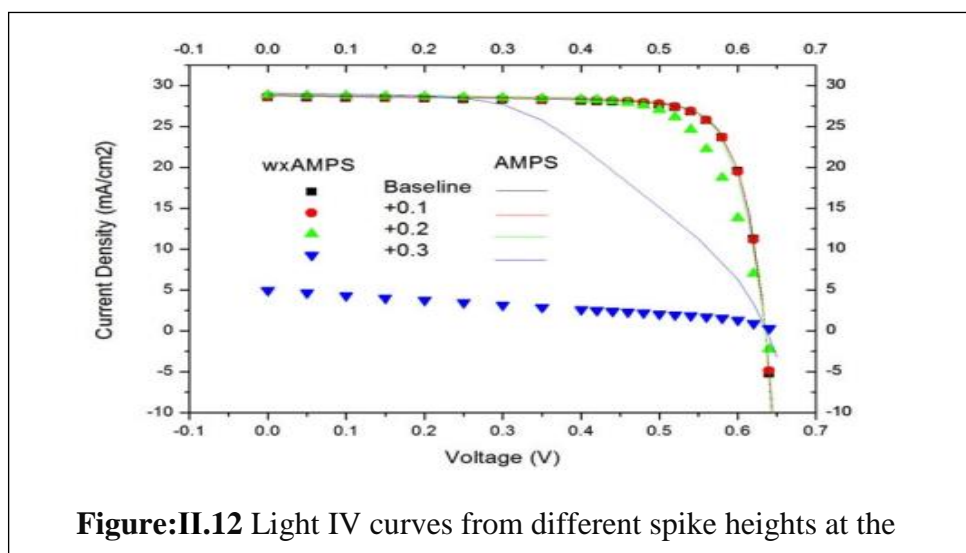
Figure:II.12 Light IV curves from different spike heights at the

As seen from the Figure II.13, the energy band diagram produced by the intra-band model shows noticeable discontinuities between *Efn*and*Efp*at the hetero junction, especially a significant discontinuity of 0.6 eV for the *Efp*, whereas in the drift-diffusion model quasi-Fermi levels at interfaces are the same.

The comparisons show that when simulating abrupt hetero junction solar cells with a high band spike, thermionic emission limits will take effect and cause significant differences among these models.
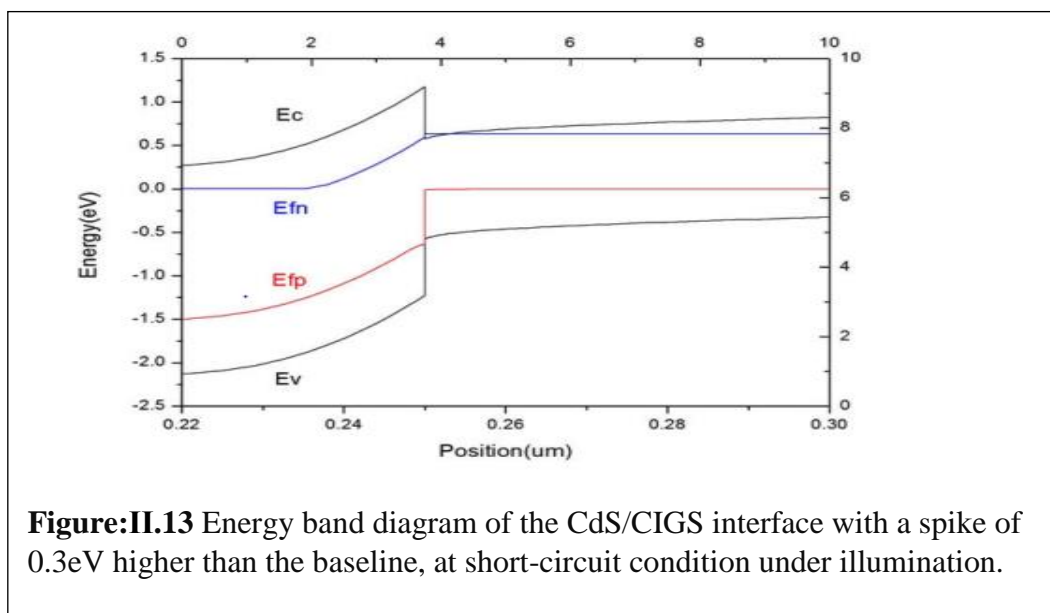
Figure:II.13 Energy band diagram of the CdS/CIGS interface with a spike of 0.3eV higher than the baseline, at short-circuit condition under illumination.

II.4 Conclusion

In this chapter, we presented the properties of the materials (Si) (CZTSS), and we also presented some concepts about the program wxAMPS3.

In the next and final chapter, we will simulate two cells in shape tandem.

Chapter III :
Results and discussion

III.1 Introduction

Due to the high costs of the experiments, the researchers resorted to simulations that allow us to predict the operation of electronic devices and in this work we will study a tandem solar cell based on CZTSSe / Si using a 1D program: wxAMPS 1D under AM1.5 illumination.

First, we have studied each cell separately to ensure the correct functioning of the two cells before we put them into tandem structure.

III.2 CZTSS Solar Cell

III.2.1 Cell Structure

The cell structure consists of a window and a transparent layer FTO (type n), a barrier layer CdS (type n), and an absorbent layer $CZTS_{1-Y}Se_Y$, as shown in the figure (III.1).Parameters are shown in the table(III.1). In this work we dida simulation of CZTSS cell and we tested the effect of the gap energy Eg (ev) and the thickness (x)of CZTSS layer on cell parameters . The program also shows us the (I.V) property, which is shownon figure(III.2).

FigureIII.1: CZTSS Solar CellStructure
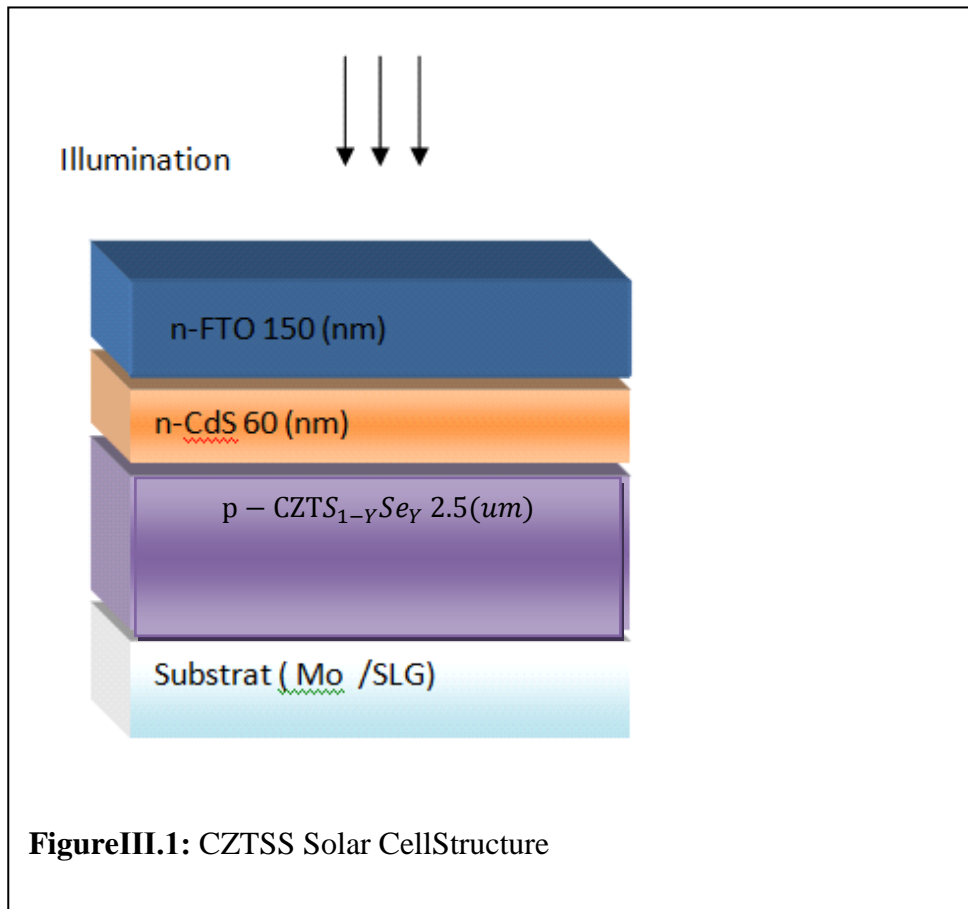
Table (III.1): the parametre of a solar cell CZTSSe

	FTO	CdS	CZTSS
Permittivity	10	10	10
Eg(ev)	4.2	2.4	1.5
Affinity(ev)	4.5	4.2	4.2
Nc(cm^{-3})	1.2×10^{20}	2.2×10^{18}	2.2×10^{18}
Nv(cm^{-3})	7×10^{20}	1.8×10^{19}	1.8×10^{19}
µn(cm²/v/s)	2×10	1×10^{2}	1×10^{2}
µp(cm²/v/s)	1×10^{2}	2.5×10	2.5×10
Nd(cm^{-3})	1×10^{20}	1×10^{17}	0
Na(cm^{-3})	0	1	2×10^{16}

Voc :0.9807 V
Jsc :19.3914 mA/cm2
FF :82.7258 %
Effi:15.7328 %
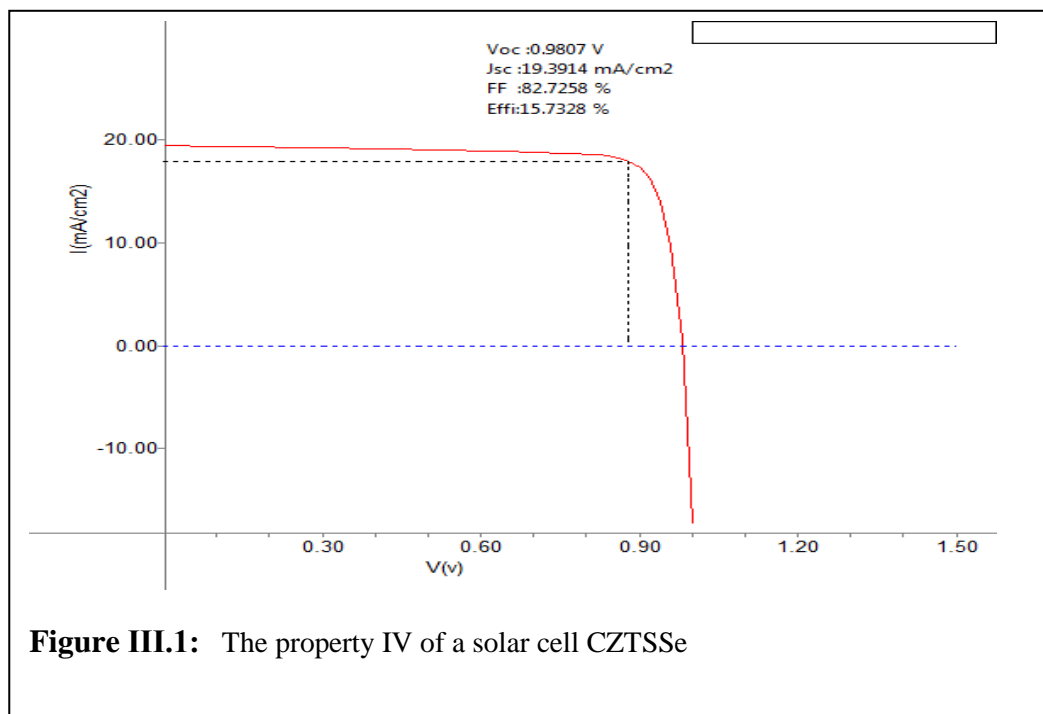
Figure III.1:   The property IV of a solar cell CZTSSe

III.2.2 The effect of thickness on CZTSS

We havestarted our study by changing the thickness and fixing Eg =1.5 which gavesthe results shown ontable(III.1),and curves.

TableIII.2 : Table showing the effect of $CZTS_{1-Y}Se_Y$ layer thickness

Thikness(µm)	Voc(V)	Jsc(mA/cm²)	FF(%)	Ƞ(%)
1	0.9754	19.2136	82.2084	15.4074
1.5	0.98	19.427	82.563	15.7194
2	0.9806	19.409	82.6936	15.7388
2.5	0.9507	19.3914	82.7285	15.7328
3	0.9808	19.395	82.7309	15.7373
3.5	0.9808	19.4097	82.7288	15.7493
4	0.9808	19.4189	82.7265	15.7565
4.5	0.9808	19.4162	82.7265	15.7543
5	0.9808	19.4097	82.7269	15.749

Curve III.1: curve showing the effect of $CZTS_{1-Y}Se_Y$ layer thickness on open circuit voltageVoc(V)
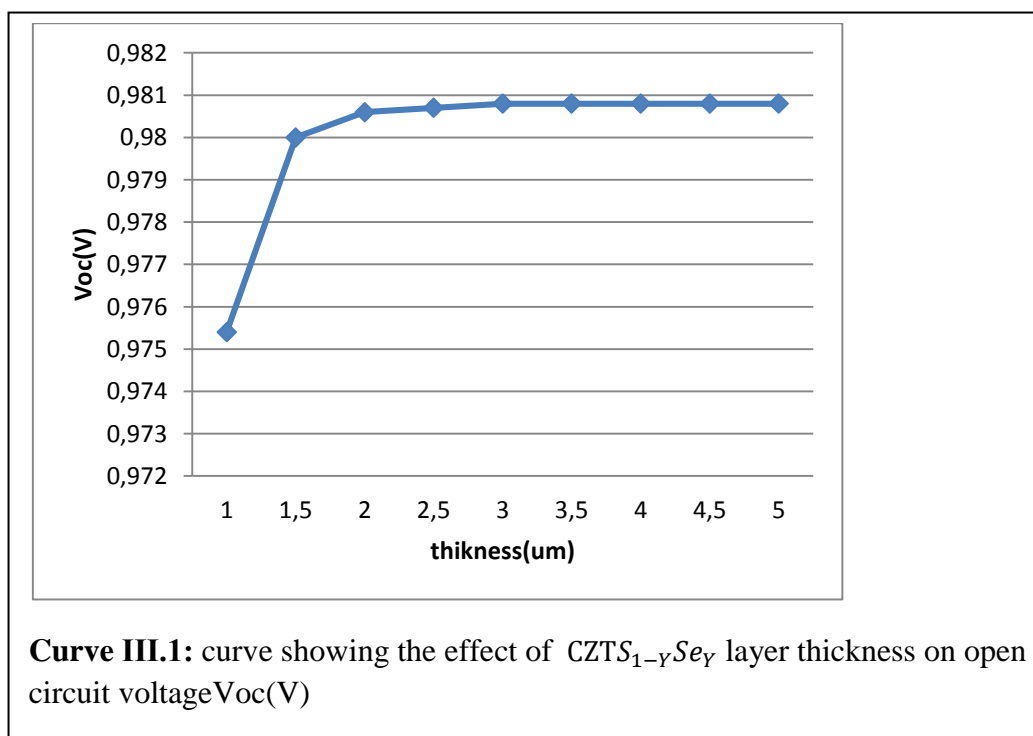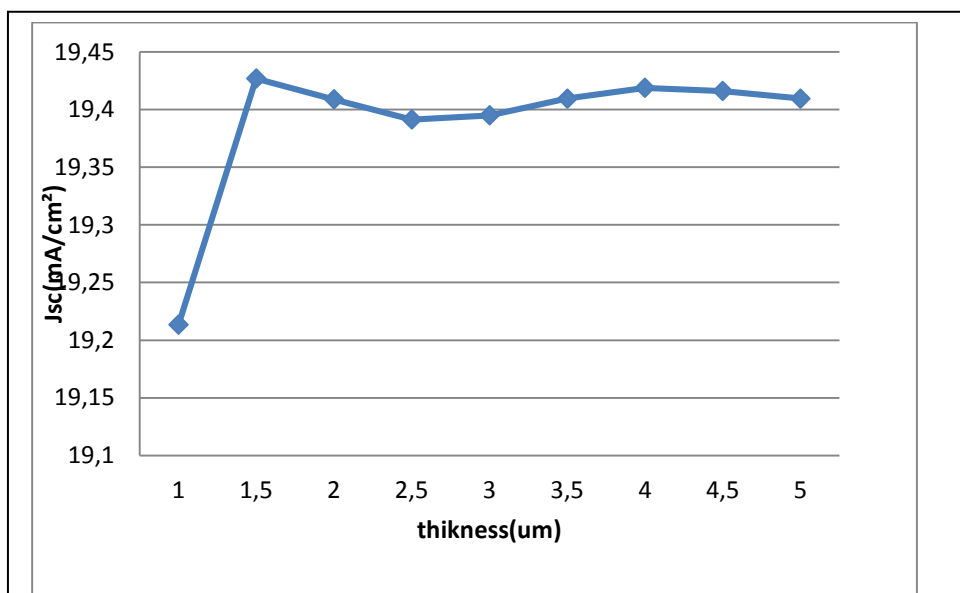
Curve III.2 curve showing the effect of $CZTS_{1-Y}Se_Y$ layer thickness on the short circuit density Jsc(mA/cm²)
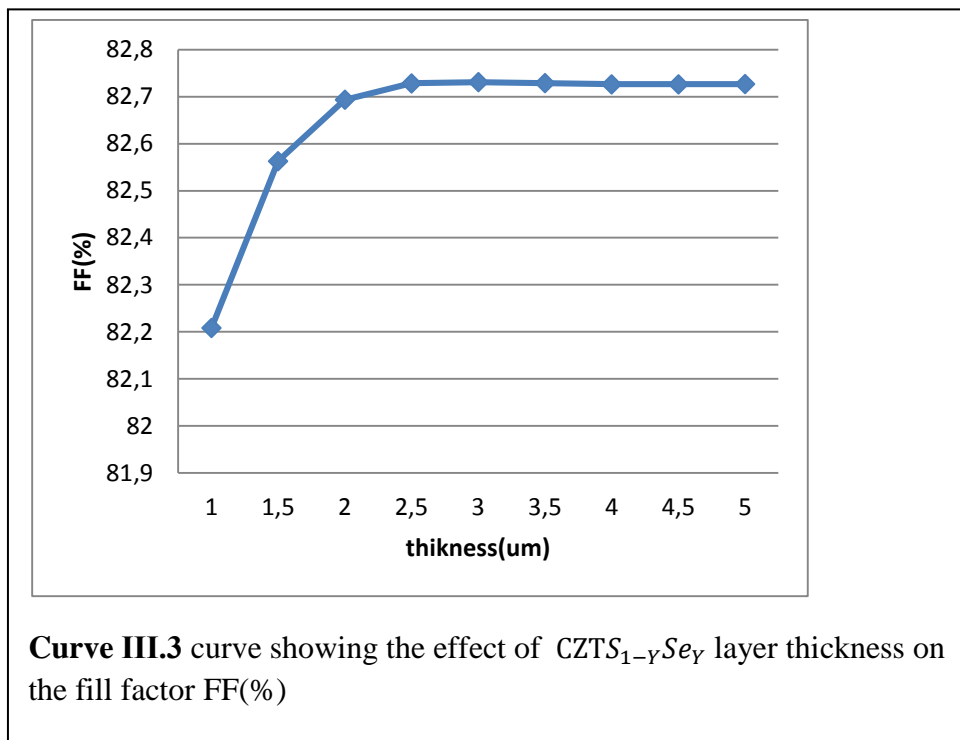
Curve III.3 curve showing the effect of $CZTS_{1-Y}Se_Y$ layer thickness on the fill factor FF(%)

Curve III.4: curve showing the effect of $CZTS_{1-Y}Se_Y$ layer thickness on efficiency QE(%)
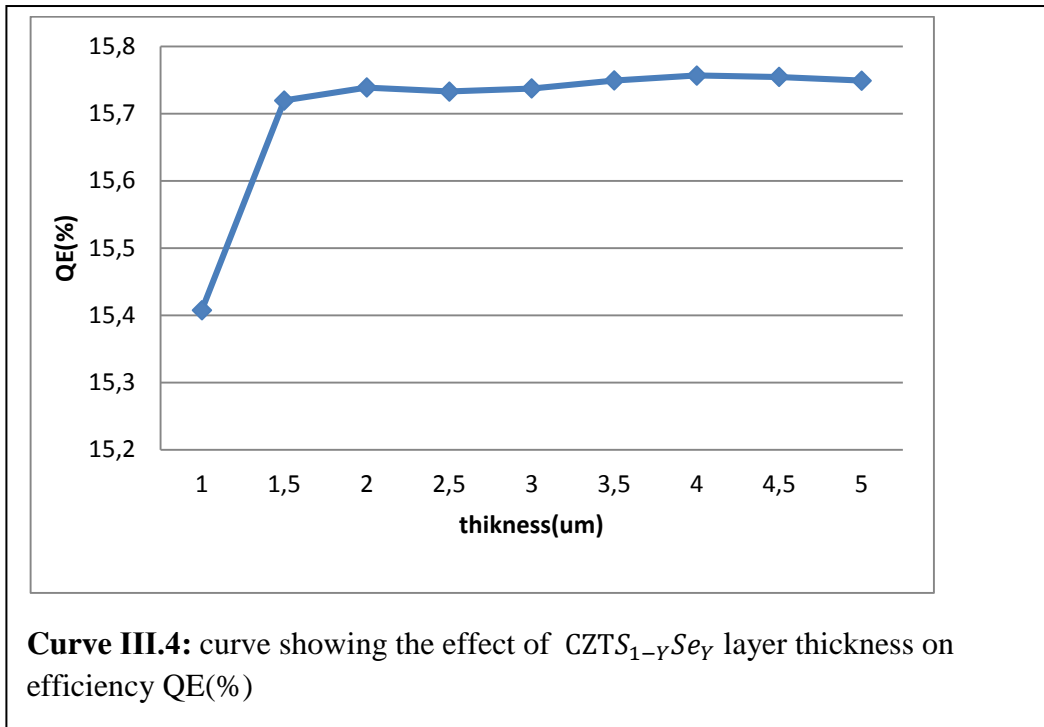
We note that the thickness of the absorbent layer slightly affects Voc, Jsc, FF and QE ,however,the efficiency is fixed at a value of 15% because the thickness does not significantly affect the absorption of photons,so 2.5um should be set as the appropriate thickness.

III.2.3 Effect of band energy on CZTSS

It is well known that The changeofselenium concentration in the compound leads toa change in the band-gap energy. To calculate the gap energy as a function of the concentration y we used this formula :

$$Eg(y) = 1.505(1 - y) + 0.984y - 0.123x(1 - y)$$

After running the simulation, we observed a difference in (IV) curve such that the band-gap energy is variable knowing that the thickness takes a constant value 2.5um , as it is shown on Table (III.3) and curves.

Table III.3 Table showing the effect of band energy on CZTSS

Thikness CZTSS=2.5µm				
Eg(ev)	Voc(V)	Jsc(mA/cm²)	FF(%)	η(%)
1.1	0,5807	19,0961	78,0295	8,6535
1.15	0,6294	19,1406	79,0639	9,5244
1.2	0,6807	19,1825	79,5208	10,3841
1.25	0,7294	19,2221	80,1551	11,2882
1.3	0,7807	19,2595	80,8497	12,1572
1.35	0,8294	19,295	81,5611	13,0519
1.4	0,8807	19,3288	81,9152	13,945
1.45	0,9294	19,3609	82,3401	14,8157
1.5	0,9807	19,3914	82,7258	15,7328
1.55	1,0294	19,4206	83,0909	16,6107
1.6	1,0807	19,4485	83,3567	17,5207
1.65	1,1294	19,4752	83,7301	18,4162
1.7	1,1807	19,5008	83,857	19,3085

Curve III.5: showing the effect of the energy band on open circuit voltageVoc(V)
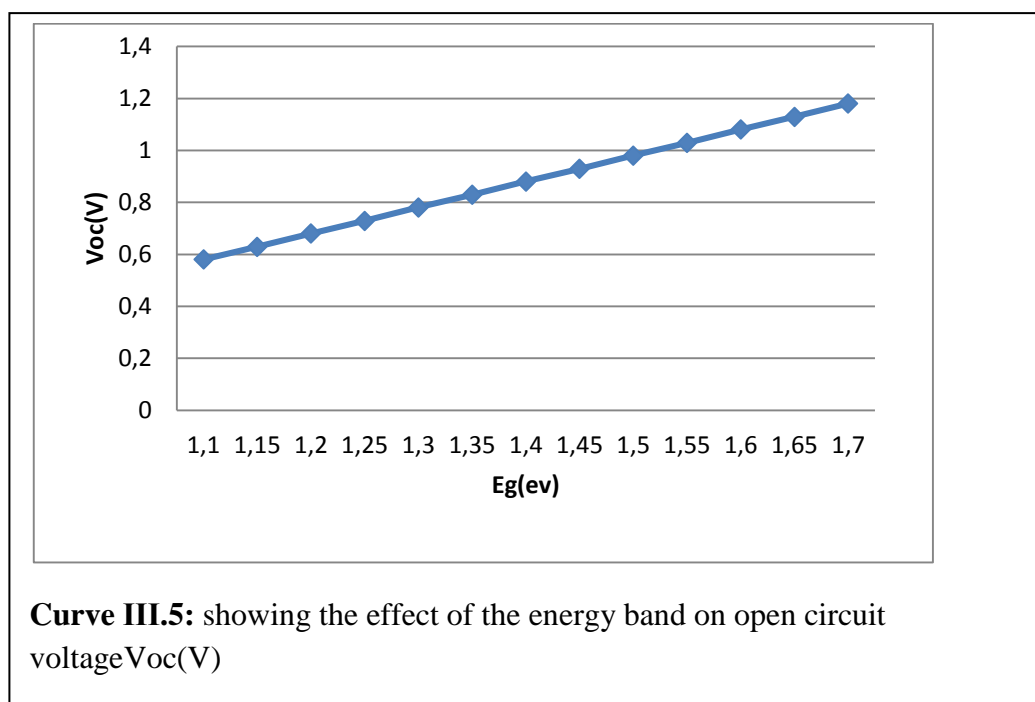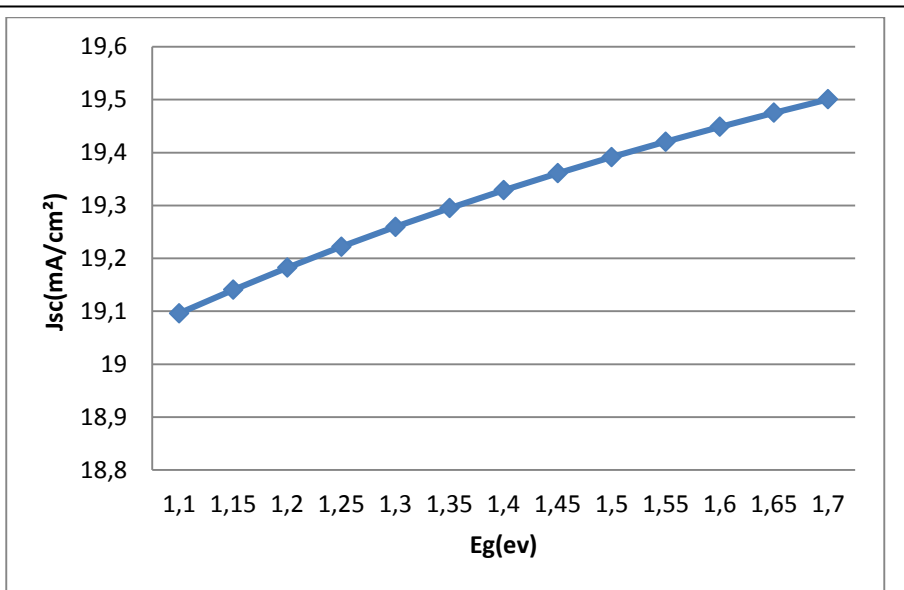
Curve III.6: showing the effect of the energy band on short circuit density Jsc(mA/cm²)
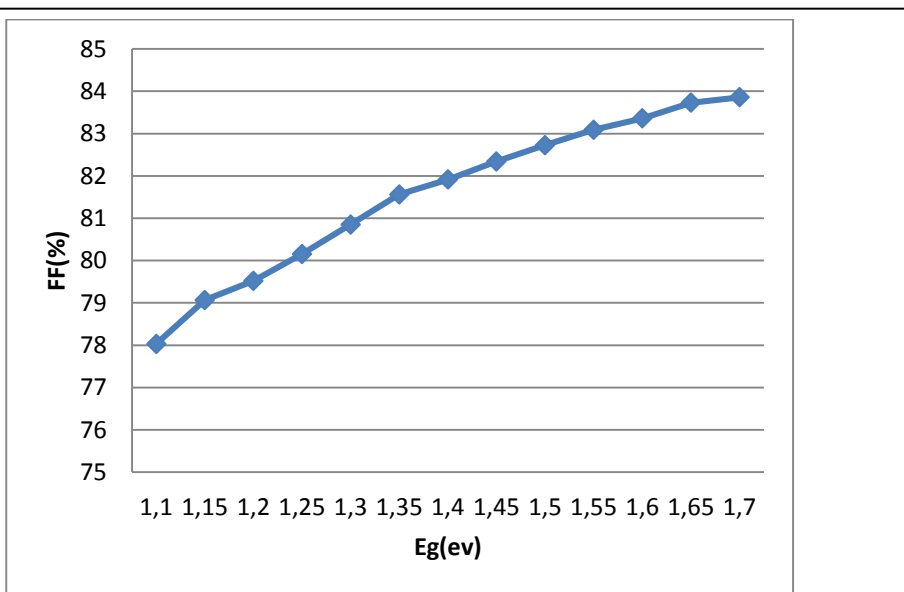
CurveIII.7: showing the effect of the energy band on fill factor FF(%)

Curve III.8: showing the effect of the energy band on efficiency QE
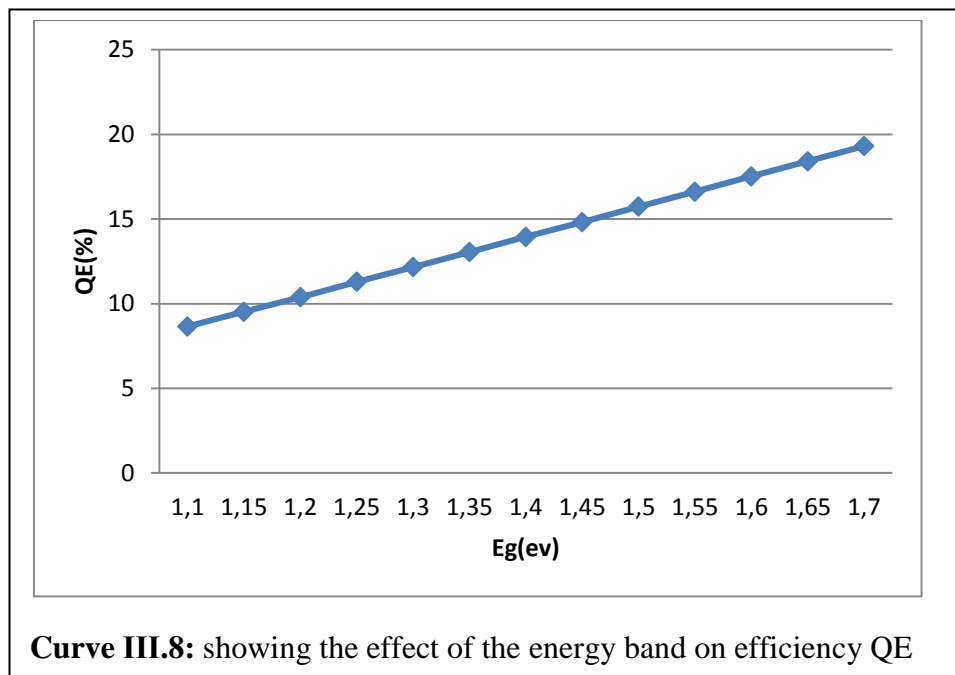
From these results we note a continuous increase in the open circuit voltage(Voc), short circuit current (Jsc), fill factor (FF) and efficiency(QE) from 8 to 19%. This happened due to the absorption's increasing of high-energy photons in proportion to the increase of Eg.

III.3 Si solar cell

III.3.1 Cell Structure

As shown on figure (III.4),The silicon cell used in oursimulationis monocrystalline (Eg=1.12 ev). We can not use polycrystalline silicon because ofits band gap (1.8 eV). CellParameters are shown in the table(III.4),and the property (IV) is shown in figure(III.5).
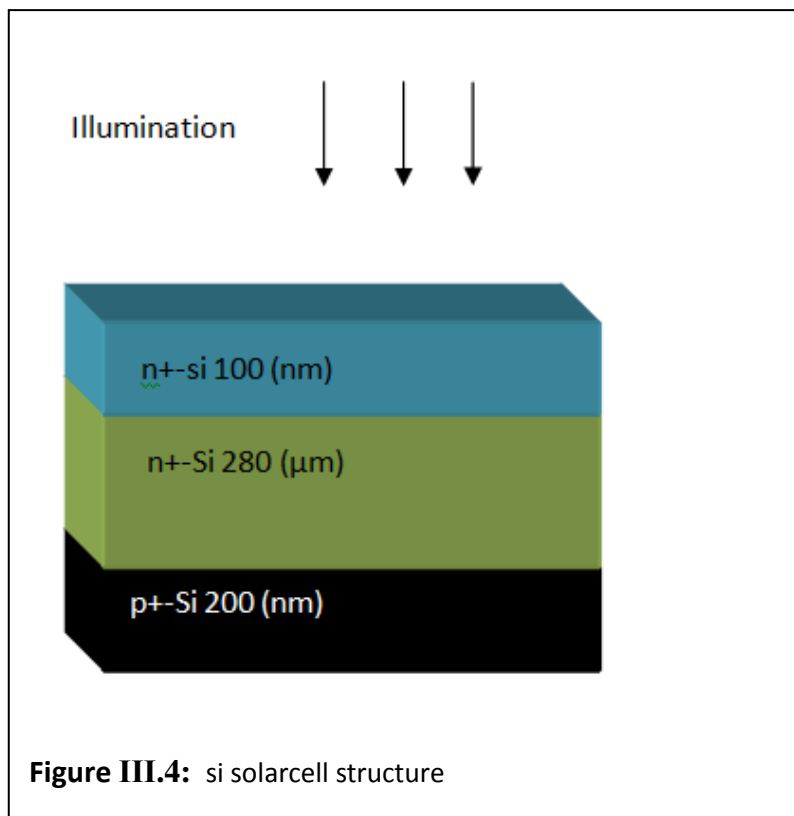
Figure III.4: si solarcell structure

Table III.4: Table showing silicone cell parameters

	Si-n+	Si-p	Si-p+
Permittivity	11.9	11.9	11.9
Eg(ev)	1.12	1.12	1.12
Affinity(ev)	4.05	4.05	4.05
$Nc(cm^{-3})$	2.8×10^{19}	2.8×10^{19}	2.8×10^{19}
$Nv(cm^{-3})$	2.6×10^{19}	2.6×10^{19}	2.6×10^{19}
µn (cm²/v/s)	1350	1350	1350
µp(cm²/v/s)	480	480	480
$Nd(cm^{-3})$	1×10^{18}	0	0
$Na(cm^{-3})$	0	1×10^{16}	1×10^{20}
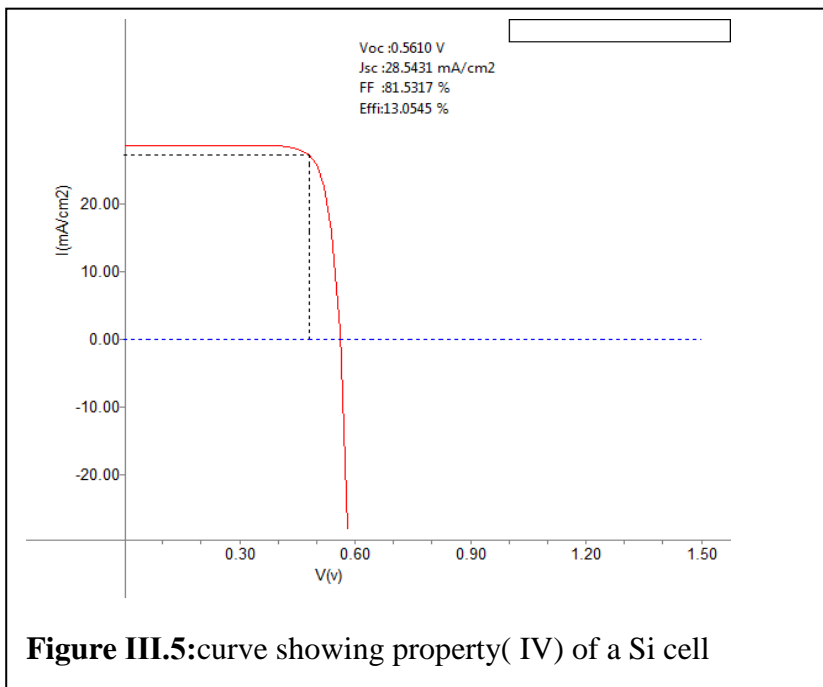
Figure III.5:curve showing property(IV) of a Si cell

Table III.5: A table showing the results for a Si cell

Solarcell	Voc(V)	Jsc(mA/cm²)	FF(%)	η(%)
Si	0.5610	28.5431	81.5317	13.0545

III.4 Tandemcell

III.4.1 Cell structure

We installed a tandem cell consisting of a top cell CZTS (Eg = 1.5 EV) and abottom cell si (Eg = 1.12 EV) to divide the solar spectrum where the top cell absorbs high energy photons (small wavelength) and low energy photons (large wavelength) absorbed by the bottom cell From the tandem cell, the structure of the tandem cell is shown in Figure (III.6)
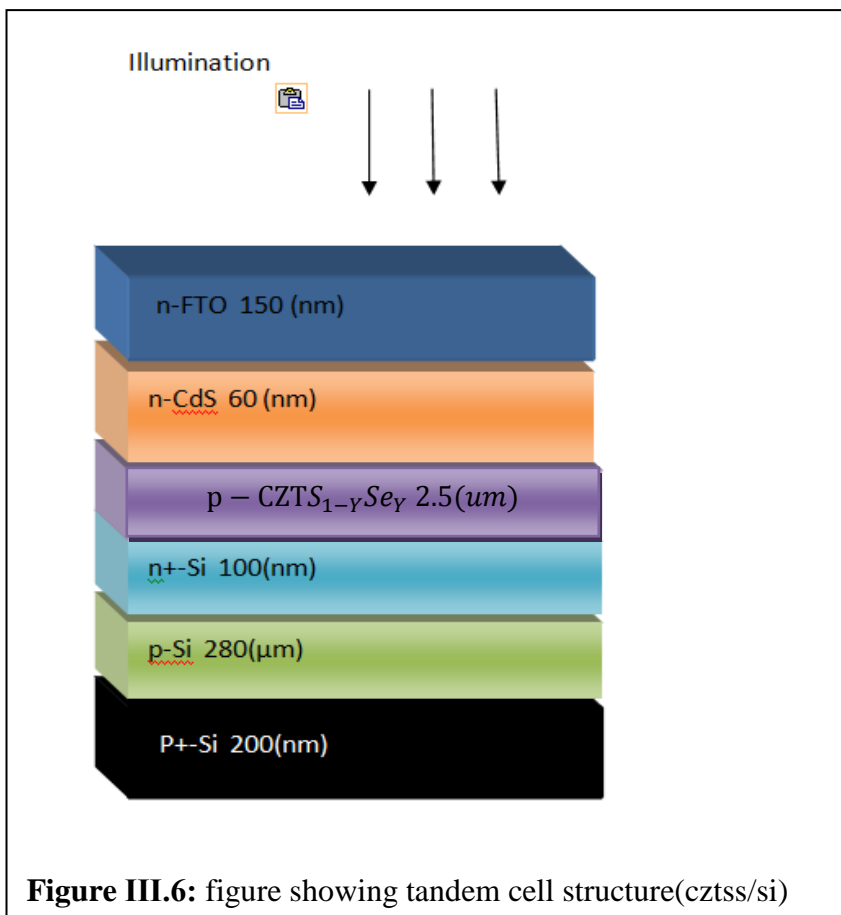
Figure III.6: figure showing tandem cell structure(cztss/si)
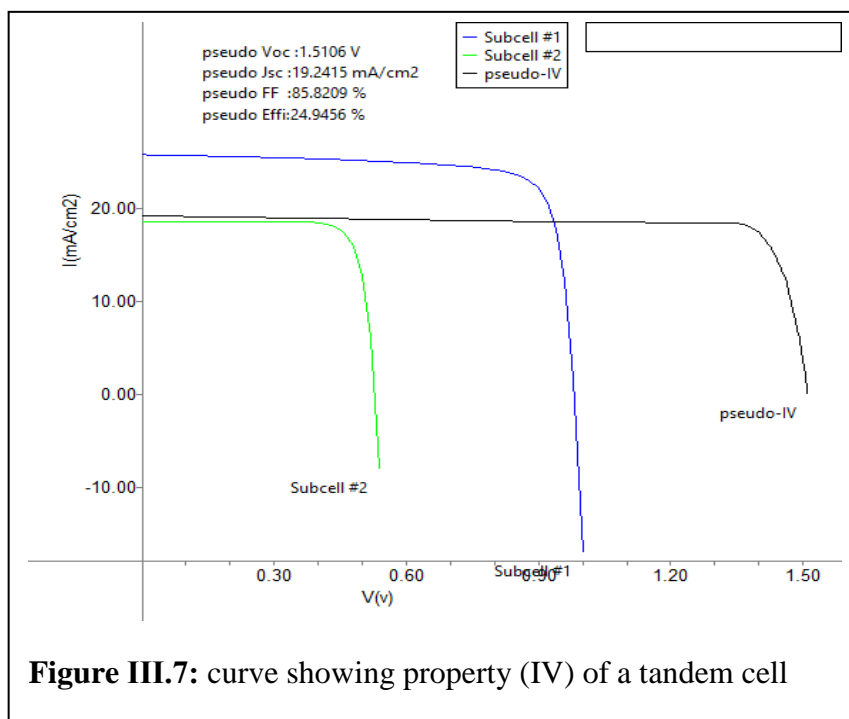
Figure III.7: curve showing property (IV) of a tandem cell

Table III.5: A table showing the results for a tandem cell

cell	Voc(V)	Jsc(mA/cm²)	FF(%)	η(%)
Tandem	1,5106	19,2415	85,8209	24,9456

III.4.2 Comparison of result

We can clearly Noticethat Voc, Jsc, FF, and QEofthe tandem cell are greater than those of each cells separately. Results are shown in a table (III.6) :

Table III.6 : Table showing a tandem cell comparison with two separate cells

Solarcell	Voc(V)	Jsc(mA/cm²)	FF(%)	η(%)
CZTS	0,9807	19,3914	82,7258	15,7328
Si	0.5610	28.5431	81.5317	13.0545
Tandemcell	1,5106	19,2415	85,8209	24,9456

III.4.3 Effect of band energy on CZTSSe tandem

After the result obtained previously of tandem cell(Eg CZTS = 1.5eV) , we have studied the effect of changing Eg ofCZTSSe and we set thickness at 2.5um.Obtained resultsare shown ontable(III.7) andcurves :

Table III.7: Table showing the effect of increasing the band-gap energy

Eg(eV)	Voc(V)	Jsc(mA/cm²)	FF%	QE%
1	1,0107	18,9434	82,8138	15,8553
1,1	1,1107	19,003	83,7263	17,6713
1,2	1,2107	19,0626	84,4507	19,4899
1,3	1,3107	19,1223	85,0206	21,3085
1,4	1,4106	19,1819	85,4692	23,127
1,5	1,5106	19,2415	85,8209	24,9456
1,6	1,6106	19,3012	86,0995	26,7657
1,7	1,7106	19,3608	86,3833	28,6092
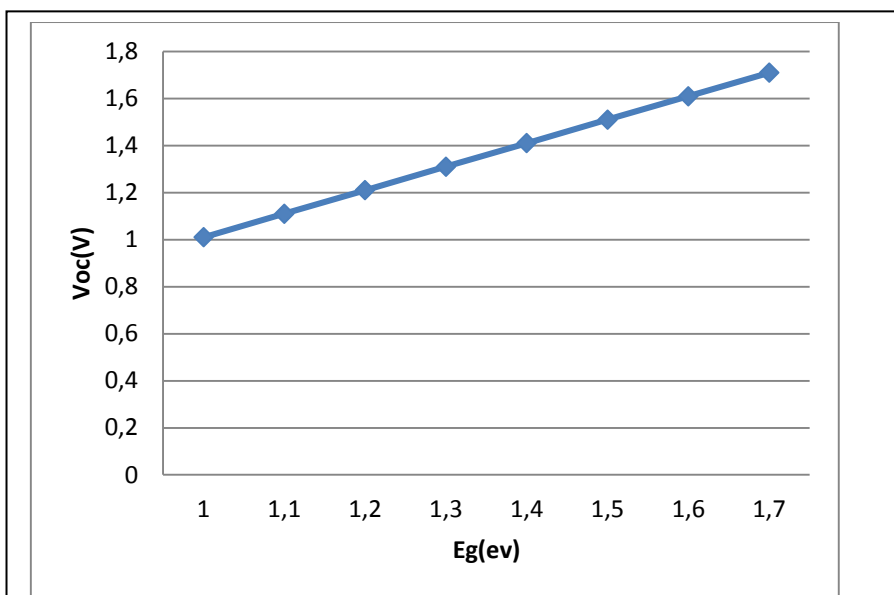
Curve III.9 : curve showing the effectof tandem cell band energy on open circuit voltage Voc(V)
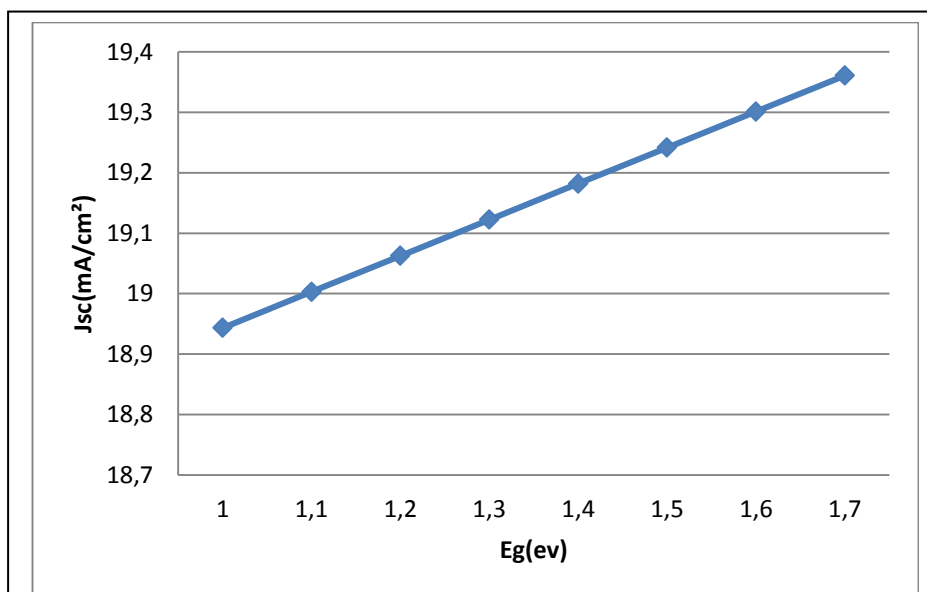
Curve III.10: curve showing the effectof tandem cell band energy on short circuit densityJsc(mA/cm²)

Curve III.11:curve showing the effectof tandem cell band energy on fill factor FF(%)

Curve III.12: curve showing the effectof tandem cell band energy on efficiency QE(%)
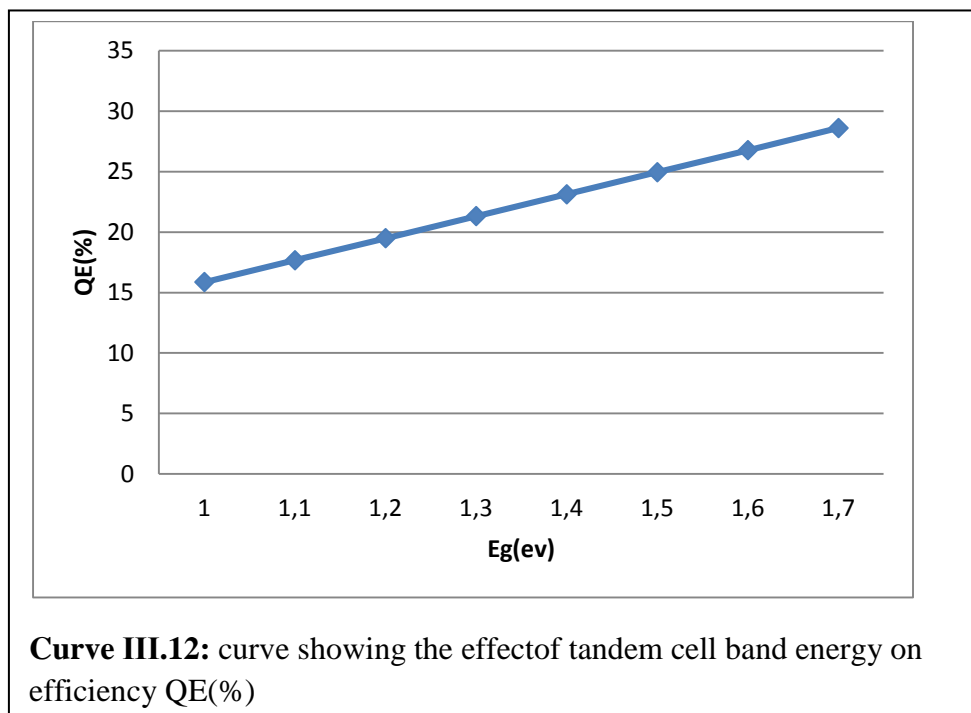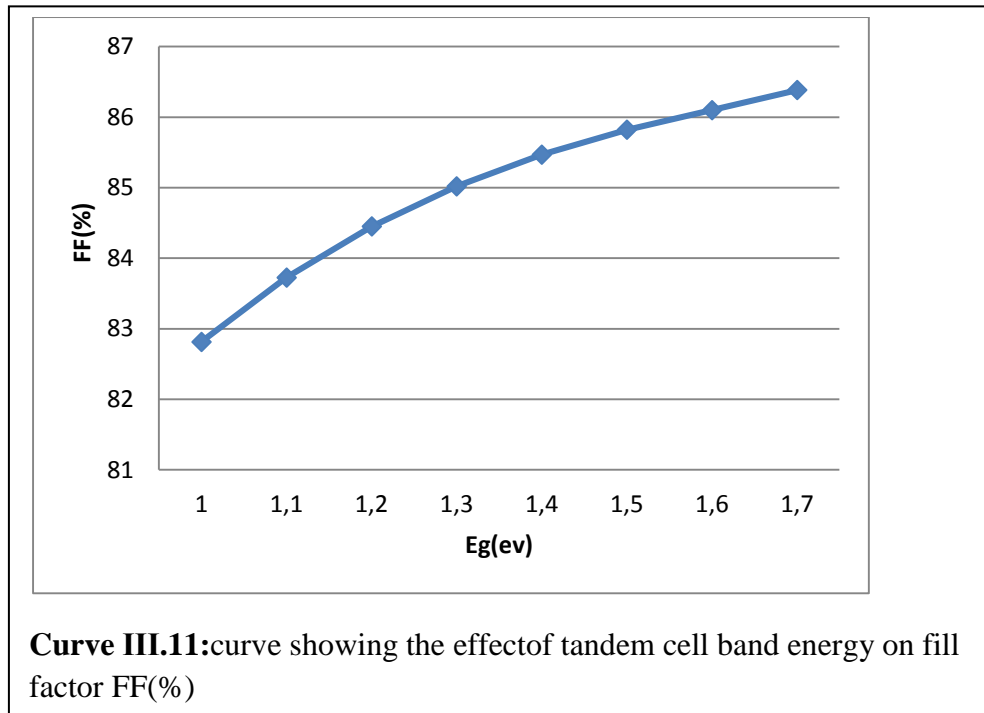
The results presented in the table (III.7) show that the higher the gap energy values the better the parameters of the tandem increase in the open circuit voltage (Voc), short circuit current(Jsc),fill factor(FF) and efficiency (QE), reaching its maximum value 28,60%. This means that it is desirable to use the largest possible Eg of CZTSSe absorber layer.

In fact, if we look at the equation used in this work (wich links Eg with ratio of selenium)we notice the largest possible value for Eg is 1.5eV. This means that Eg changes from 1 to 1.5 eV

only, but in our simulation we have expanded the range of energy change to 1.7 Ev. Because recent papers proved that Egof KesteriteCZTSSe compounds can reach a value of 1.7Ev.

III.4 Conclusion

After we simulated a tandem solar cell based on CZTSSe / Si, we got good results, reaching 28%, while in cells si and cztsse we got 13% and 19%, respectively.

This is the aim of the studies that have come out to improve a silicon solar cell.

Conclusion general

In this thesis the results of a tandem cztsse / si solar cell simulation by wxAMPS3 program are given.

First, the cztsse solar cell was simulated by wxAMPS3 software. We studied The effect of energy range on the cell and we observed a significant increase in cell efficiency from 15.75 to 19% while studying the effect of thickening, we noted that it does not affect effectively This is due to the thickness of the cell. It does not significantly affect absorption Photons.

Second, a solar cell is simulated by the same program and we get 13% efficiency. Then we fixed the two cells into the tandem structure, where the cztsse cell is The upper cell and the Si lower ring cell in order to study the effect of a Eg energy on the CZTSSe / Si tandem cell until it reached 28.60%.

Finally the results obtained from the simulation were discussed, and we found that Tandem cells give the best efficiency to individual cells, which is what it is due to the solar spectrum split, and this was our goal to improve the silicon cell. This message dealt with a type of tandem cell that was mentioned previously. As discussed above in general, the simulation results in this message showed good results compared to what this type of tandem cells can give. This message also gives a comprehensive idea about CZTS / Si tandem solar cells as well as about CZTS cell alone. These results prove that this technology, i.e. tandem cell technology, can be developed from any side to give a very high efficiency.

References

[1] NREL (2014) Reference Solar Spectral Irradiance: ASTM G-173. National Renewable Energy
Laboratory. Available at http://rredc.nrel.gov/solar/spectra/ (accessed 10 July 2014).

[2]. E. Becquerel (1839). "Mémoire sur les effets électriques produits sous
l'influence des rayons solaires". *Comptes Rendus* **9**: 561–567. Issue date: May [7], 1935.

[3]. http://en.wikipedia.org/wiki/Timeline_of_solar_cells

[4]. W.G. Adams and R.E. Day (1877) "The action of light on selenium" in
Proceedings of the Royal Society, A25, 113.

[5]. David C. Brock (Spring 2006). "Useless No More: Gordon K. Teal,
Germanium, and Single-Crystal Transistors". *Chemical Heritage
Newsmagazine* (Chemical Heritage Foundation) **24** (1). Retrieved 2008-01-21.

[6]. Bloch, F, Z. Phys. (1928), 52, 555.

[7]. Wilson, A. H., Proc. Roy. Soc. A (1931), 133, 458; 134, 277.

[8]. Gerald L. Pearson, Daryl M. Chapin, and Calvin S. Fuller(AT&T) receive
patent US2780765, "*Solar Energy Converting Apparatus*."(1957)

[9]. http://en.wikipedia.org/wiki/Telstar

[10]. Alferov, Zh. I., V. M. Andreev, M. B. Kagan, I. I. Protasov, and V. G. Trofim, 1970,
''Solar-energy converters based on p-n AlxGa12xAs-GaAs heterojunctions,'' Fiz.
Tekh. Poluprovodn. 4, 2378 (Sov. Phys. Semicond. 4, 2047 (1971))

[11]. http://en.wikipedia.org/wiki/Public_Utility_Regulatory_Policies_Act

[12]. Lewis Fraas, James Avery, James Gee, Keith Emery, et. al., "Over 35%
Efficient GaAs/GaSb Stacked Concentrator Cell Assemblies for Terrestrial
Applications", 21st IEEE PV Specialist Conference, p. 190 (1990).

[13]. Friedman D et al., Prog. Photovolt.: Res. Appl. 3, 47–50 (1995)

[14]. Lewis Fraas, Russ Ballantyne, She Hui, Shi-Zhong Ye, Sean Gregory, Jason
Keyes, James Avery, David Lamson, Bert Daniels, "Commercial GaSb cell and
circuit development for the Midnight Sun® TPV stove" AIP Conference
Proceedings 03/1999; 460(1):480-487. DOI:10.1063/1.57830

[15]. http://en.wikipedia.org/wiki/German_Renewable_Energy_Act

[16]. K Araki et al, A 28 % Efficient, 400 X & 200 WP Concentrator
...,www.physics.usyd.edu.au/app/solar/.../pdf/19thEUPV_5BV_2_20.pdf

[17]. PVPS_report_-_A_Snapshot_of_Global_PV_-_1992-2013_-_final_3.pdf;
http://en.wikipedia.org/wiki/Agua_Caliente_Solar_Project

[18] .https://en.wikipedia.org/wiki/Semiconductor

[19] .https://www.pveducation.org/pvcdrom/pn-junctions/semiconductor-materials

[20] .https://www.pveducation.org/pvcdrom/pn-junctions/semiconductor-structure

[21]. https://www.pveducation.org/pvcdrom/pn-junctions/band-gap

[22].file:///C:/Users/home/Downloads/@Adrian%20Kitai%20Principles%20of%20Solar%20Cell
s,%20LEDs%20and%20Diodes%20The%20role%20of%20the%20PN%20junction%20%20201
1%0(1).pdf

[23].file:///D:/PV%20LightHouse/Crystalline%20Silicon%20Solar%20Cells%20by%20Adolf%2
0Goetzberger,%20Joachim%20Knobloch,%20Bernhard%20Voss%20(z-lib.org)%20-%20Copie-
12039486603.pdf

[24] .file:///C:/Users/home/Downloads/NOUVO1551828963(1).PDF

[25]. https://en.wikipedia.org/wiki/Extrinsic_semiconductor#N-type_semiconductors

[26]. https://en.wikipedia.org/wiki/Extrinsic_semiconductor#P-type_semiconductors

[27]. https://en.wikipedia.org/wiki/P%E2%80%93n_junction

[28] .https://www.pveducation.org/pvcdrom/pn-junctions/doping

[29]. ^ a b Solar Cells. chemistryexplained.com

[30] .^ "Solar cells – performance and use". solarbotic s.net.

[31]. P.Würfel,Physics of Solar Cells(WILEY-VCHVerlag,Weinheim,Germany,2005).

[32].Green MA, Emery K, Hishikawa Y, Warta W, Dunlop ED. Solar cell efficiency tables (Version 48). Progress in Photovoltaics: Research and Applications 2016;

[33].M. Wu, X. Lin, Y. Wang, L. Wang, W. Guo, D. Qi, X. Peng, A. Hagfeldt, M. Grätzel, T. Ma, J. Am. Chem. Soc. 2012, 134, 3419–3428.

[34]. A. Fakharuddin, R. Jose, T. M. Brown, F. F. Santiago, J. Bisquert, Energy Environ. Sci. 2014, 7,3952–3981.

[35] E. D. Jackson. In *Transaction of Conference on use of Solar Energy, Tucson 1955*, volume 5,pages 122–125. U. of Arizona Press, 1958.

[36] A. S. Brown and M. A. Green. Detailed balance limit for the series constrained two terminal tandem solar cell. *Physica E*, **14**:96–100, 2002.

[37]. B. Burnett. 2002. The Basic Physics and Design of III-V Multijunction Solar Cells. National Renewable Energy Laboratory. Golden, CO. [Online]. Available: photo chemistry.epfl.ch/EDEY/NREL.pdf

[38] N. Yastrebova, April 2007, High-efficiency multi-junction solar cells: Current status and future potential. University of Ottawa. Ottawa, Canada. [Online]. Available: http://sunlab.site.uottawa.ca/pdf/whitepapers/HiEfficMjSc-CurrStatus&FuturePotent ial.pdf

[39] M. Wolf. (1960, July). Limitations and Possibilities for Improvement of Photovoltaic Solar Energy Converters, Part 1. Proc. IRE. 48(7) [Online] pp. 1246-1263. Available: http://ieeexplore.ieee.org/xpls/abs_all.jsp?arnumber=4066168

[40] S. Kurtz. (2011, June). Opportunities and Challenges for Development of Mature Concentrating Photovoltaic Power Industry. National. Renewable Energy Laboratory, Golden, CO. [Online]. Available: http://www.nrel.gov/docs/fy11osti/43208.pdf

[41] A. Hermle, G. Letay, S. P. Philipps, and A. W. Bett. Numerical simulation of tunnel diodes for multi-junction solar cells. *Progress in Photovoltaics*, **16**(5):409–418, 2008.

[42] K. Jandieri, S. D. Baranovskii, W. Stolz, and F. Gebhard. Analytical theory for favorable defects in tunnel diodes. *Journal of Applied Physics*, **104**(11):114511, 2008.

[43] Jeffrey F. Wheeldon, Christopher E. Valdivia, Alexandre W. Walker, Gitanjali Kolhatkar, Abdelatif Jaouad, Artur Turala, Bruno Riel, Denis Masson, Norbert Puetz, Simon Fafard, Richard Ares, Vincent Aimez, Trevor J. Hall, and Karin Hinzer. Performance comparison of AlGaAs, `GaAs and InGaP tunnel junctions for concentrated multijunction solar cells. *Progress in Photovoltaics*, pages 442–452, Nov 2010.

[44] H. Sugiura, C. Amano, A. Yamamoto, and M. Yamaguchi. Double heterostructure GaAs tunnel junction for a AlGaAs/GaAs tandem solar-cell. *Japanese Journal Of Applied Physics Part 1-Regular Papers Brief Communications & Review Papers*, **27**(2):269–272, 1988.

[45] T. Takamoto, M. Yamaguchi, E. Ikeda, T. Agui, H. Kurita, and M. Al-Jassim. Mechanism of Zn and Si diffusion from a highly doped tunnel junction for InGaP/GaAs tandem solar cells. *Journal of Applied Physics*, **85**(3):1481–1486, 1999.

[46]Canham LT. Silicon quantum wire array fabrication by electrochemical and chemical dissolution of wafers. Appl. Phys. Lett. 1990;57:1046.

[47] Belomoin G, Therrien J, Smith A, Rao S, Chaieb S, Nayfeh MH. Observation of a magic discrete family of ultra bright, Si nanoparticles. Appl. Phys. Lett. 2002;80:841.

[46] Greenwood and Earnshaw, p. 330–331

[47] "Silicon Commodities Report 2011" *(PDF). USGS. Retrieved 2011-10-20*

[48] Zulehner et al., p. 574

[49] Audi, G.; Kondev, F. G.; Wang, M.; Huang, W. J.; Naimi, S. (2017). "The NUBASE2016 evaluation of nuclear properties" (PDF). Chinese Physics C. 41 (3): 030001. Bibcode:2017ChPhC..41c0001A. doi:10.1088/1674-1137/41/3/030001.

[50] Greenwood and Earnshaw, pp. 331–335

[51] Green M. A,, Proc. 10th EC PV Solar Energy Con$, Lissabon, Portugal, 1991, p. 250

[52] Knobloch, J., GlUnz S. W., Biro D., Warta W., Schaffer E. and Wettling W., Proc. 25th IEEE PVSpec. ConJ, Washington, DC, USA, 1996, p. 405

[53]https://www.pveducation.org/pvcdrom/design-of-silicon-cells/optical-losses

[54] K. Ito and Nakazawa, T., "Electrical and Optical Properties of Stannite-Type Quaternary Semiconductor Thin Films", *Japanese Journal of Applied Physics*, vol. 27, no. Part 1, No. 11, pp. 2094 - 2097, 1988.

[55]H. Katagiri, Sasaguchi, N., Hando, S., Hoshino, S., Ohashi, J., and Yokota, T., "Preparation and evaluation of Cu2ZnSnS4 thin films by sulfurization of E-B evaporated precursors", *Solar Energy Materials and Solar Cells*, vol. 49, pp. 407 - 414, 1997.

[56]T. Magorian Friedlmeier, Wieser, N., Walter, T., Dittrich, H., and Schock, H. W., "Heterojunctions based on Cu2ZnSnS4 and Cu2ZnSnSe4 thin films", in *14th European PVSEC*, 1997.

[57].H. Katagiri *et al.*, "Development of CZTS-based thin film solar cells", *Thin Solid Films*, vol. 517, pp. 2455–2460, 2009.

[58] Q. Guo, Hillhouse, H. W., and Agrawal, R., "Synthesis of Cu$_2$ZnSnS$_4$ Nanocrystal Ink and Its Use for Solar Cells", *Journal of the American Chemical Society*, vol. 131, no. 33, pp. 11672 - 11673, 2009.

[59] file:///C:/Users/Home/Downloads/a%20CZTSSe%20results.pdf

[60] K.-L. Ou, J.-C. Fan, J.-K. Chen, C.-C. Huang, L.-Y. Chen, J.-H. Ho, et al., J. Mater. Chem. 22 (2012) 14667.

[61] W. Ki, H.W. Hillhouse, Adv. Energy Mater. 1 (2011) 732

[62] J. Heyd , G. E. Scuseria , *J. Chem. Phys.* **2004**, *121*, 1187 .

[63] L. Hedin , *Phys. Rev.* **1965**, *139*, A796 .

[64] E. N. Brothers , A. F. Izmaylov , J. O. Normand , V. Barone ,
G. E. Scuseria , *J. Chem. Phys.* **2008**, *129*, 011102 .

[65] J. P. Perdew , M. Levy , *Phys. Rev. Lett.* **1983**, *51*, 1884 .

[66] S. Chen , A. Walsh , J. H. Yang , X. Gong , L. Sun , P. X. Yang , J. H. Chu ,
S. H. Wei , *Phys. Rev. B* **2011**, *83*, 125201

[67] S. B. Zhang , S.-H. Wei , A. Zunger , *Phys. Rev. Lett.* **2000**, *84*, 1232

[68] A. Walsh , C. R. A. Catlow , M. Miskufova , A. A. Sokol , *J. Phys.: Condens. Matter* **2011**, *23*, 334217 .

[69] Y.-H. Li , A. Walsh , S. Chen , W.-J. Yin , J.-H. Yang , J. Li ,
J. L. F. Da Silva , X. G. Gong , S.-H. Wei , *Appl. Phys. Lett.* **2009**, *94*,
 212109

[70] J. Jaffe , A. Zunger , *Phys. Rev. B* **1984**, *29*, 1882 .

[71] D.B. Mitzi, O. Gunawan, T.K. Todorov, K. Wang, S. Guha, Sol. Energy Mater. Sol. Cells 95 (2011) 1421.

[72] I. Repins, N. Vora, C. Beall, S.-H. Wei, Y. Yan, M. Romero, et al., Mater. Res. Soc. (2011) April 2529, San Francisco, CA.

[73] S. Chen, X.G. Gong, A. Walsh, S.-H. Wei, Appl. Phys. Lett. 92 (2010) 0121902.

[74] K. Ito, Copper zinc tin sulphide-based thin film solar cells. John Wiley & Sons, Ltd (2015).

[75] G.Altamura. Development of CZTSSe thin films based solar cells, Material chemistry. Universit´e Joseph-Fourier - Grenoble I (2014).

[76] J.J.Scragg, P.J.Dale, & L. M. Peter, Thin Solid Films, 517, 2481–2484(2009).

[77] K.Ito, & T.Nakazawa, Japanese Journal of Applied Physics, 27, 2094–2097(1988).

[78]V.G. Rajeshmon, C.S. Kartha, K.P. Vijayakumar, C. Sanjeeviraja, T. Abe, Y. Kashiwaba, Sol. Energy 85 (2011) 249

[79] M. Kumar, Dubey, A., Adhikari, N., Venkatesan, S., and Qiao, Q., "Strategic review of secondary phases, defects and defect-complexes in kesterite CZTS–Se solar cells"**,** *Energy Environ. Sci.*, vol. 8, no. 11, pp. 3134 - 3159, 2015.

[80].T. Gokmen, Gunawan, O., Todorov, T. K., and Mitzi, D. B., "Band tailing and efficiency limitation in kesterite solar cells"**,** *Applied Physics Letters*, vol. 103, p. 103506, 2013.

[81]C. J. Hages, Carter, N. J., and Agrawal, R., "Generalized quantum efficiency analysis for non-ideal solar cells: Case of $Cu_2ZnSnSe_4$"**,** *Journal of Applied Physics*, vol. 119, no. 1, p. 014505, 2016.

[82] C. J. Hages, Koeper, M. J., and Agrawal, R., "Optoelectronic and material properties of nanocrystal-based \{CZTSe\} absorbers with Ag-alloying", *Solar Energy Materials and Solar Cells*, vol. 145, Part 3, pp. 342 - 348, 2016.

[83] F. Hong, Lin, W., Meng, W., and Yan, Y., "Trigonal Cu_2-II-Sn-VI_4 (II = Ba, Sr and VI = S, Se) quaternary compounds for earth-abundant photovoltaics", *Phys. Chem. Chem. Phys.*, vol. 18, no. 6, pp. 4828 - 4834, 2016.

[84] Q. Guo, H.W. Hillhouse, R. Agrawal, J. Am. Chem. Soc. 131 (2009) 11673.

[85] T. Todorov, O. Gunawan, S.J.W Chey, T.G. Monsabert, A. Prabhakar, D.B. Mitzi, Thin Solid Films 519 (2011) 7378.

[86] Y. Liu, D. Heinzel, and A. Rockett, "A revised version of the AMPS simulation code", in Photovoltaic Specialists Conference (PVSC), 2010 35th IEEE, 2010, pp. 001943-001947.

[87] S. Fonash, et al., "A Manual for AMPS-1D for Windows 95/NT", The Pennsylvania State University, 1997.

[88] K. Yang, "Modeling of abrupt heterojunctions using a thermionic-field emission boundary conditions", SolidState Electronics, vol. 36, issue 3, pp. 321-330, 1993.

[89] M. Gloeckler, "NUMERICAL MODELING OF CIGS AND CdTe SOLAR CELLS_SETTING THE BASELINE", 3rd conference on photovoltaic energy conversion, 2003.

[90] G. A. M. Hurkx, D. B. M. Klaassen, and M. P. G. Knuvers, "A new recombination model for device simulation including tunneling", Electron Devices, IEEE Transactions on, vol. 39, pp. 331-338, 1992.

[91] https://wiki.engr.illinois.edu/display/solarcellsim/.